

# Delving into the Devils of Bird's-eye-view Perception: A Review, Evaluation and Recipe

Hongyang Li<sup>\*†</sup>, Chonghao Sima<sup>\*</sup>, Jifeng Dai<sup>\*</sup>, Wenhai Wang<sup>\*</sup>, Lewei Lu<sup>\*†</sup>, Huijie Wang<sup>\*</sup>,  
Enze Xie<sup>\*</sup>, Zhiqi Li<sup>\*</sup>, Hanming Deng<sup>\*</sup>, Hao Tian<sup>\*</sup>, Xizhou Zhu, Li Chen, Yulu Gao,  
Xiangwei Geng, Jia Zeng, Yang Li, Jiazhi Yang, Xiaosong Jia, Bohan Yu,  
Yu Qiao, Dahua Lin, Si Liu, Junchi Yan, Jianping Shi and Ping Luo

**Abstract**—Learning powerful representations in bird's-eye-view (BEV) for perception tasks is trending and drawing extensive attention both from industry and academia. Conventional approaches for most autonomous driving algorithms perform detection, segmentation, tracking, etc., in a front or perspective view. As sensor configurations get more complex, integrating multi-source information from different sensors and representing features in a unified view come of vital importance. BEV perception inherits several advantages, as representing surrounding scenes in BEV is intuitive and fusion-friendly; and representing objects in BEV is most desirable for subsequent modules as in planning and/or control. The core problems for BEV perception lie in (a) how to reconstruct the lost 3D information via view transformation from perspective view to BEV; (b) how to acquire ground truth annotations in BEV grid; (c) how to formulate the pipeline to incorporate features from different sources and views; and (d) how to adapt and generalize algorithms as sensor configurations vary across different scenarios. In this survey, we review the most recent work on BEV perception and provide an in-depth analysis of different solutions. Moreover, several systematic designs of BEV approach from the industry are depicted as well. Furthermore, we introduce a full suite of practical guidebook to improve the performance of BEV perception tasks, including camera, LiDAR and fusion inputs. At last, we point out the future research directions in this area. We hope this report will shed some light on the community and encourage more research effort on BEV perception. We keep an active repository to collect the most recent work and provide a toolbox for bag of tricks at <https://github.com/OpenPerceptionX/BEVPerception-Survey-Recipe>.

**Index Terms**—Autonomous Driving, Bird's-eye-view (BEV) Representation, 3D Detection and Segmentation, Waymo Open Challenge.

## 1 INTRODUCTION

PERCEPTION recognition task in autonomous driving is essentially a 3D geometry reconstruction to the physical world. As the diversity and number of sensors become more and more complicated in equipping the self-driving vehicle (SDV), representing features from different views in a unified perspective comes to vital importance. The well-known bird's-eye-view (BEV) is a natural and straightforward candidate view to serve as a unified representation. Compared to its front-view or perspective view counterpart, which is broadly investigated [1, 2] in 2D vision domains, BEV representation bears several inherent merits. First, it has no occlusion or scale problem as commonly existent in 2D tasks. Recognizing vehicles with occlusion or cross-traffic could be better resolved. Moreover, representing objects or road elements in such form would favorably make it convenient for subsequent modules (e.g. planning, control) to develop and deploy.

In this survey, we term **BEV Perception** to indicate all

vision algorithms in sense of the BEV view representation for autonomous driving. Note that we do not intend to exaggerate BEV perception as a new research concept; instead, how to formulate new pipeline or framework under BEV view for better feature fusion from multiple sensor inputs, deserves more attention from the community.

### 1.1 Big Picture at a Glance

Based on the input data, we divide BEV perception research into three parts mainly - BEV camera, BEV LiDAR and BEV fusion. Fig. 1 depicts the general picture of BEV perception family. Specifically, **BEV camera** indicates vision-only or vision-centric algorithms for 3D object detection or segmentation from multiple surrounding cameras; **BEV LiDAR** describes detection or segmentation task from point cloud input; **BEV fusion** depicts the fusion mechanisms from multiple sensor inputs, such as camera, LiDAR, GNSS, odometry, HD-Map, CAN-bus, etc.

As described in Fig. 1, we group and classify fundamental perception algorithms (classification, detection, segmentation, tracking, etc.) with autonomous driving tasks into three levels, where the concept of BEV perception lies in the middle. Based on different combinations from the sensor input layer, fundamental task, and product scenario, a certain BEV perception algorithm could indicate accordingly. For instance, M<sup>2</sup>BEV [3] and BEVFormer [4] belonged to BEV camera track from multiple cameras to perform multiple tasks including 3D object detection and BEV map segmentation. BEVFusion [5] devised a fusion strategy in BEV

- This is a joint work from Shanghai AI Laboratory and SenseTime Research. \*indicates equal contribution. For detailed role of each author, please refer to Author Contributions section. <sup>†</sup>Primary contact to: Dr. Hongyang Li [lihongyang@pjlab.org.cn](mailto:lihongyang@pjlab.org.cn) or Dr. Lewei Lu [luotto@sensetime.com](mailto:luotto@sensetime.com). Author Contribution is listed in Appendix
- H. Li, C. Sima, J. Dai, W. Wang, H. Wang, Z. Li, X. Zhu, L. Chen, Y. Gao, X. Geng, J. Zeng, Y. Li, J. Yang, X. Jia, Y. Qiao and D. Lin are with Shanghai AI Laboratory. L. Lu, H. Deng, H. Tian, B. Yu and J. Shi are with SenseTime Research. E. Xie and P. Luo are with University of Hong Kong; S. Liu is with Beihang University; J. Yan is with Shanghai Jiao Tong University.

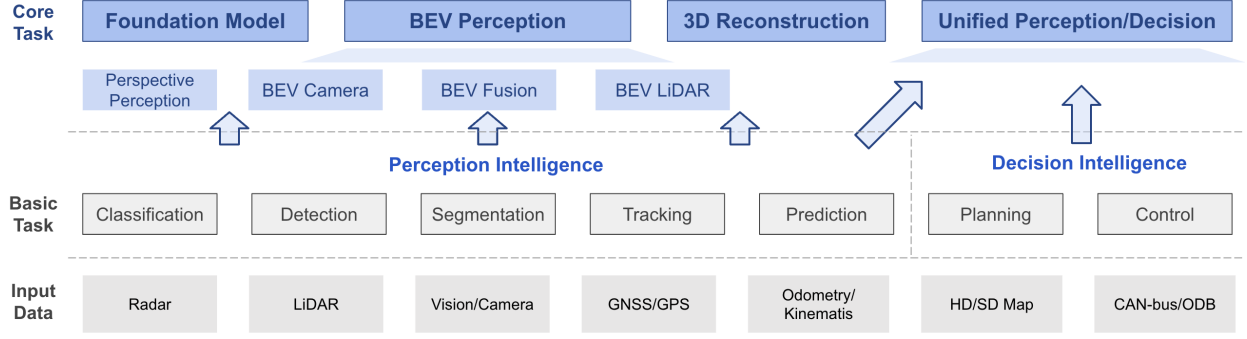


Fig. 1: The general picture of BEV perception at a glance, where consists of three sub-parts based on the input modality. BEV perception is a general task built on top of a series of fundamental tasks. For better completeness of the whole perception algorithms in autonomous driving, we list other topics (e.g., Foundation Model) as well.

space to perform 3D detection and tracking simultaneously from both camera and LiDAR inputs. Tesla [6] released its systematic pipeline to detect objects and lane lines in vector space (BEV) for L2 highway navigation and smart summon. In this report, we aim to summarize a general pipeline and key insights for recent advanced BEV perception research, apart from various input combinations and tasks.

## 1.2 Motivation to BEV Perception Research

When it comes to the motivation of BEV perception research, three important aspects need to be examined.

**Significance.** *Will BEV perception generate a real and meaningful impact on academia and/or society?* It is well-known that there is a tremendous performance gap between camera or vision based solutions over LiDAR or fusion based counterparts. For example, as of submission in August 2022, the gap of first-ranking method between vision-only vs LiDAR is over 20% in terms of NDS on nuScenes dataset [7]. The gap is even more than 30% on Waymo benchmark [8]. This naturally motivates us to investigate whether or not the vision solutions can beat or be on par with the LiDAR approaches.

From the academic perspective, the very essence of designing a camera-based pipeline such that it outperforms LiDAR, is better to understand the view transformation process from a 2D, appearance input to a 3D, geometry output. How to transfer camera features into geometry representations as does in point cloud leaves a meaningful impact for the academic society. On the industrial consideration, the cost of a suite of LiDAR equipment into SDV is expensive; OEMs (Original Equipment Manufacturer, e.g., Ford, BMW, etc.) prefer a cheap as well as accurate deployment for software algorithms. Improving camera-only algorithms to LiDAR’s naturally fall into this goal since the cost of a camera is usually 10x times cheaper than LiDAR. Moreover, camera based pipeline can recognize long-range distance objects and color-based road elements (e.g., traffic lights), both of which LiDAR approaches are incapable of.

Although there are several different solutions for camera and LiDAR based perception, BEV representation is one of the best candidates for LiDAR based methods in terms of superior performance and industry-friendly deployment. Moreover, recent trends show that BEV representation also has huge progress for multi-camera inputs. Since camera

and LiDAR data can be projected to BEV space, another potential for BEV is that we can easily fuse the feature from different modalities under a unified representation.

**Space.** *Are there open problems or caveats in BEV perception that require substantial innovation?* The gist behind BEV perception is to learn a robust and generalizable feature representation from both camera and LiDAR inputs. This is easy in LiDAR branch as the input (point cloud) bears such a 3D property. This is non-trivial otherwise in the camera branch, as learning 3D spatial information from monocular or multi-view settings is difficult. While we see there are some attempt to learn better 2D-3D correspondence by pose estimation [9] or temporal motion [10], the core issue behind BEV perception requires a substantial innovation of depth estimation from raw sensor inputs, esp. for the camera branch.

Another key problem is how to fuse features in early or middle stage of the pipeline. Most sensor fusion algorithms treat the problem as a simple object-level fusion or naive feature concatenation along the blob channel. This might explain why some fusion algorithms behave inferior to LiDAR-only solutions, due to the misalignment or inaccurate depth prediction between camera and LiDAR. How to align and integrate features from multi-modality input plays a vital role and thereby leaves extensive space to innovate.

**Readiness.** *Are key conditions (e.g. dataset, benchmark) ready to conduct BEV perception research?* The short answer is yes. As BEV perception requires both camera and LiDAR, high-quality annotation and accurate alignment between 2D and 3D objects are two key evaluations for such benchmarks. While KITTI [11] is comprehensive and draws much attention in early autonomous driving research, large-scale and diverse benchmarks such as Waymo [8], nuScenes [7], Argoverse [12] provide a solid playground for validating BEV perception ideas. These newly proposed benchmarks usually feature high-quality labels; the scenario diversity and data amount also scale up to great extent. Furthermore, open challenges [13] on these leaderboards give a fair setting on the held-out test data, where all state-of-the-arts can be compared in an open and prompt sense.

As for the algorithm readiness, recent years have witnessed a great blossom for general vision, where Transformer [14], ViT [15, 16], Masked Auto-encoders (MAE) [17] and CLIP [18], etc., achieve impressive gain over conven-

tional methods. We believe these work would benefit and inspire greatness for of BEV perception research.

Based on the discussions of the three aspects above, we conclude that BEV perception research has great potential impact, and deserves massive attention from both academia and industry to put great effort for a long period. Compared to the recent surveys on 3D object detection [19, 20, 21, 22, 23], our survey not only summarizes recent BEV perception algorithms at a more high level and formulates them into a general pipeline, but also provides useful recipe under such context, including solid data augmentation in both camera-based and LiDAR-based settings, efficient BEV encoder design, perception heads and loss function family, useful test-time augmentation (TTA) and ensemble policy, and so on. We hope this survey can be a good starting point for new beginners and an insightful discussion for current researchers in this community.

### 1.3 Contributions

The main contributions in this survey are three-fold.

- 1) We review the whole picture of BEV perception research in recent years, including high-level philosophy and in-depth detailed discussion.
- 2) We elaborate on a comprehensive analysis of BEV perception literature. The core issues such as depth estimation, view transformation, sensor fusion, domain adaptation, etc., are covered. Several important industrial system-level designs for BEV perception are introduced and discussed as well.
- 3) We provide a practical cookbook, besides theoretical contribution, for improving the performance in various BEV perception tasks. Such a release could facilitate the community to achieve better performance in a grab-and-go recipe sense.

## 2 BACKGROUND IN 3D PERCEPTION

In this section, we present the essential background knowledge in 3D perception. In Sec. 2.1, we review conventional approaches to perform perception tasks, including monocular camera based 3D object detection, LiDAR based 3D object detection and segmentation, and sensor fusion strategies. In Sec. 2.2, we introduce predominant datasets in 3D perception, such as KITTI dataset [11], nuScenes dataset [7] and Waymo Open Dataset [8].

### 2.1 Task Definition and Related Work

**Monocular Camera-based Object Detection.** Monocular camera-based methods take an RGB image as input and attempt to predict the 3D location and category of each object. The main challenge of monocular 3D detection is that the RGB image lacks depth information, so these kinds of methods need to predict the depth. Due to estimating depth from a single image being an ill-posed problem, typically monocular camera-based methods have inferior performance than LiDAR-based methods.

**LiDAR Detection and Segmentation.** LiDAR describes surrounding environments with a set of points in the 3D space, which capture geometry information of objects. Despite the

lack of color and texture information and the limited perception range, LiDAR-based methods outperform camera-based methods by a large margin due to the depth prior.

**Sensor Fusion.** Modern autonomous vehicles are equipped with different sensors such as cameras, LiDAR and Radar. Each sensor has advantages and disadvantages. Camera data contains dense color and texture information but fails to capture depth information. LiDAR provides accurate depth and structure information but suffers from limited range and sparsity. Radar is more sparse than LiDAR, but has a longer sensing range and can capture information from moving objects. Ideally, sensor fusion would push the upper bound performance of the perception system, and yet how to fuse data from different modalities remains a challenging problem.

### 2.2 Datasets and Metrics

We introduce some popular autonomous driving datasets and the common evaluation metrics. Tab. 1 summarizes the main statistics of prevailing benchmarks for BEV perception. Normally, a dataset consists of various scenes, each of which is of different length in different datasets. The total duration ranges from tens of minutes to hundreds of hours. For BEV perception tasks, 3D bounding box annotation and 3D segmentation annotation are essential and HD-Map configuration has become a mainstream trend. Most of them can be adopted in different tasks. A consensus reached that sensors with multiple modes and various annotations are required. More types of data [7, 12, 24, 25, 33, 39] are released such as IMU/GPS and CAN-bus. Similar to the Kaggle and EvalAI leaderboards, we reveal the total number of submissions on each dataset to indicate the popularity of a certain dataset.

#### 2.2.1 Datasets

**KITTI Dataset.** KITTI [11] is a pioneering autonomous driving dataset proposed in 2012. It has 7481 training images and 7518 test images for 3D object detection tasks. It also has corresponding point clouds captured from the Velodyne laser scanner. The test set is split into 3 parts: easy, moderate, and hard, mainly by the bounding box size and the occlusion level. The evaluation of object detection is of two types: 3D object detection evaluation and bird's eye view evaluation. KITTI is the first comprehensive dataset for multiple autonomous driving tasks, and it draws massive attention from the community.

**Waymo Dataset.** The Waymo Open Dataset v1.3 [8] contains 798, 202 and 80 video sequences in the training, validation, and testing sets, respectively. Each sequence has 5 LiDARs and 5 views of side left, front left, front, front right and side right image resolution is  $1920 \times 1280$  pixels or  $1920 \times 886$  pixels. Waymo is large-scale and diverse. It is evolving as the dataset version keeps updating. Each year Waymo Open Challenge would define new tasks and encourage the community to work on the problems.

**nuScenes Dataset.** The nuScenes Dataset [7] is a large scale autonomous driving dataset which contains 1000 driving scenes in two cities. 850 scenes are for training/validation and 150 are for testing. Each scene is 20s long. It has 40k keyframes with entire sensor suite including 6 cameras,

TABLE 1: BEV perception datasets at a glance. **Scenes** means clips of dataset and the length of scene is varying for diverse datasets. Under **City**, “AS” for Asia, “EU” for Europe, “NA” for North America, “Sim” for simulation data. Under **Sensor Data**, “Scans” for point cloud. Under **Annotation**, **Frames** means the number of 3D bbox/ 3D lane annotation frames, **3D bbox/ 3D lane** means the number of 3D bbox/ 3D lane annotation instances, **3D seg.** means the number of segmentation annotation frames of point cloud. “# Subm.” indicates the popularity of a certain dataset by the number of submissions on Kaggle. † indicates that a certain statistic is unavailable; – means that a certain field is not applicable (non-existent).

Dataset	Year	City	Sensor Data				Annotation				HD-Map	Other Data	# Subm.
			Scenes	Hours	Scans	Images	Frames	3D bbox	3D lane	3D seg.			
KITTI [11]	2012	EU	22	1.5	15k	15k	15k	80k	-	-	✗	-	380+
Waymo [8]	2019	NA	1150	6.4	230k	12M	230k	12M	-	50k	✗	-	200+
nuScenes [7]	2019	NA/AS	1000	5.5	390k	1.4M	40k	1.4M	-	40k	✓	CAN-bus	350+
Argo v1 [24]	2019	NA	113	0.6	22k	490k	22k	993k	-	-	✓	-	100+
Argo v2 [12]	2022	NA	1000	4	150k	2.7M	150k	†	-	-	✓	-	10+
ApolloScape [25]	2018	AS	103	2.5	29k	144k	144k	70k	†	-	✓	-	200+
OpenLane [26]	2022	NA	1000	6.4	-	200k	200k	-	880k	-	✗	-	-
ONCE-3DLanes [27]	2022	AS	†	†	-	211k	211k	-	†	-	✗	-	-
Lyft L5 [28]	2019	AF	366	2.5	46k	240k	46k	1.3M	-	-	✗	-	500+
A* 3D [29]	2019	AS	†	55	39k	39k	39k	230k	-	-	✗	-	-
H3D [30]	2019	NA	160	0.8	27k	83k	27k	1.1M	-	-	✗	-	-
SemanticKITTI [31]	2019	EU	22	1.2	43k	-	-	-	-	43k	✗	-	30+
A2D2 [32]	2020	EU	†	†	12.5k	41k	12.5k	43k	-	41k	✗	-	-
Cityscapes 3D [33]	2020	-	†	2.5	-	5k	5k	40k	-	-	✗	IMU/GPS	400+
PandaSet [34]	2020	NA	179	†	16k	41k	14k	†	-	60k	✗	-	-
KITTI-360 [35]	2020	EU	11	†	80k	320k	80k	68k	-	80k	✗	-	30+
Cirrus [36]	2020	-	12	†	6285	6285	6285	†	-	-	✗	-	-
ONCE [37]	2021	AS	†	144	1M	7M	15k	417k	-	-	✗	-	-
AIODrive [38]	2021	Sim	100	2.8	100k	1M	100k	26M	-	100k	✓	-	-
DeepAccident [39]	2022	Sim	464	†	131k	786k	131k	1.8M	-	131k	✓	-	-

1 LiDAR and 5 Radars. The camera image resolution is  $1600 \times 900$ . Meanwhile, corresponding HD-Map and CAN-bus data are released to explore assistance of multiple inputs. nuScenes becomes more and more popular in the academic literature as it provides a diverse multi-sensor setting; the data scale is not as large as Waymo’s, making it efficient to fast verify idea on this benchmark.

### 2.2.2 Evaluation Metrics

**LET-3D-APL.** In the camera-only 3D detection, LET-3D-APL is used as the metric instead of 3D-AP. Compared with the 3D intersection over union (IoU), the LET-3D-APL allows longitudinal localization errors of the predicted bounding boxes up to a given tolerance. LET-3D-APL penalizes longitudinal localization errors by scaling the precision using the localization affinity. The definition of LET-3D-APL is mathematically defined as:

$$\text{LET-3D-APL} = \int_0^1 p_L(r) dr = \int_0^1 \bar{a}_l \cdot p(r) dr, \quad (1)$$

where  $p_L(r)$  indicates the longitudinal affinity weighted precision value, the  $p(r)$  means the precision value at recall  $r$ , and the multiplier  $\bar{a}_l$  is the average longitudinal affinity of all matched predictions treated as  $TP$  (true positive).

**mAP.** The mean Average Precision (mAP) is similar to the well-known AP metric in the 2D object detection, but the matching strategy is replaced from IoU to the 2D center distance on the BEV plane. The AP is calculated under different distance thresholds: 0.5, 1, 2, and 4 meters. The mAP is computed by averaging the AP in the above thresholds.

**NDS.** The nuScenes detection score (NDS) is a combination of several metrics: mAP, mATE (Average Translation Error), mASE (Average Scale Error), mAOE (Average Orientation Error), mAVE (Average Velocity Error) and mAAE (Average Attribute Error). The NDS is computed by using the weight-sum of the above metrics. The weight of mAP is 5 and 1 for the rest. In the first step the  $TP_{\text{error}}$  is converted to  $TP_{\text{score}}$  as shown in Eqn. 2, then Eqn. 3 defines the NDS:

$$TP_{\text{score}} = \max(1 - TP_{\text{error}}, 0.0), \quad (2)$$

$$\text{NDS} = \frac{5 \cdot \text{mAP} + \sum_{i=1}^5 TP_{\text{score}}^i}{10}. \quad (3)$$

## 3 METHODOLOGY OF BEV PERCEPTION

In this section, we describe in great details various perspectives of BEV perception from both academia and industry. We differentiate BEV pipeline in three settings based on the input modality, namely BEV Camera (camera-only 3D perception) in Sec. 3.1, BEV LiDAR in Sec. 3.2 and BEV Fusion in Sec. 3.3, and summarize industrial design of BEV perception in Sec. 3.4.

Tab. 2 summarizes the taxonomy of BEV perception literature based on input data and task type in a chronological order. We can see that there is trending research for BEV perception published in top-tiered venues. The task topics as well as the formulation pipelines (contribution) can be various, indicating a blossom of the 3D autonomous driving community. Tab. 3 depicts the performance gain of 3D object detection and segmentation on popular leaderboards over

TABLE 2: BEV perception literature in recent years. Under **Input Modality**, “L” for LiDAR, “SC” for single camera, “MC” for multi camera, “T” for temporal information. Under **Task**, “ODet” for 3D object detection, “LDet” for 3D lane detection, “MapSeg” for map segmentation, “Plan” for motion planning, “MOT” for multi-object tracking. **Depth Supervision** means either camera-only model uses sparse/dense depth map to supervise the model, ✓ for yes, ✗ for no, - for LiDAR-input model. Under **Dataset**, “nuS” nuScenes dataset [7], “WOD” Waymo Open Dataset [8], “KITTI” KITTI dataset [11], “Lyft” Lyft Level 5 Dataset [28], “OpenLane” OpenLane dataset [26], “AV” Argoverse Dataset [24], “Carla” carla simulator [40], “SUN” SUN RGB-D dataset [41], “ScanNet” ScanNet indoor scenes dataset [42].

Method	Venue	Input Modality	Task	Depth Supervision	Dataset	Contribution
OFT [43]	BMVC 2019	SC	ODet	✗	KITTI	Feature Projection to BEV
VoxelNet [44]	CVPR 2018	L	ODet	-	KITTI	Implicit voxel grids transformed to BEV
PointPillars [45]	CVPR 2019	L	ODet	-	KITTI	Voxelization with pillars as BEV
CaDDN [46]	CPVR 2021	SC	ODet	✓	KITTI/WOD	Depth Distribution with Supervision
DfM [10]	ECCV 2022	SC	ODet	✓	KITTI	Motion to Depth to Voxel to BEV
BEVDet [47]	arXiv 2022	MC	ODet	✓	nuS	BEV space data augmentation
PETR [48]	arXiv 2022	MC	ODet	✗	nuS	Implicit BEV Pos Embed
BEVDepth [49]	arXiv 2022	MC/T	ODet	✓	nuS	Depth Correction
ImVoxelNet [50]	WACV 2022	SC/MC	ODet	✗	nuS/KITTI SUN/ScanNet	Camera Pose with Grid Sampler to BEV
M <sup>2</sup> BEV [3]	arXiv 2022	MC	ODet/MapSeg	✗	nuS	BEV Representation without Depth
PolarFormer [51]	arXiv 2022	MC	ODet/MapSeg	✗	nuS	Polar-ray Representation in BEV
BEVFormer [4]	ECCV 2022	MC/T	ODet/MapSeg	✗	nuS/WOD	Transformer for BEV feature
BEVFusion [5]	arXiv 2022	MC/L	ODet/MapSeg	-	nuS	Fusion on BEV from Camera and LiDAR
Cam2BEV [52]	ITSC 2020	MC	MapSeg	✗	Synthetic	Homo-graphic Projection to BEV
FIERY [53]	ICCV 2021	MC	MapSeg	✗	nuS/Lyft	Future Prediction in BEV space
CVT [54]	CVPR 2022	MC	MapSeg	✗	nuS	Camera Intrinsic BEV Projection
HDMaNet [55]	ICRA 2022	MC/L/T	MapSeg	-	nuS	Feature Fusion under BEV
Image2Map [56]	ICRA 2022	SC/T	MapSeg	✗	nuS/Lyft/AV	Polar-ray Transformer in BEV
LSS [57]	ECCV 2020	MC	MapSeg/Plan	✗	nuS/Lyft	First Depth Distribution
ST-P3 [58]	ECCV 2022	MC/T	MapSeg/Plan	✓	nuS/Carla	End to End P3 with Temporal Info
3D LaneNet [59]	ICCV 2019	SC	LDet	✗	OpenLane	IPM Projection to BEV space
STSU [60]	ICCV 2021	SC	LDet	✗	nuS	Query-based Centerline in BEV
PersFormer [26]	ECCV 2022	SC	LDet	✗	OpenLane	Perspective Transformer for BEV

the years. We can observe that the performance gain improves significantly in spirit of BEV perception knowledge.

### 3.1 BEV Camera

#### 3.1.1 General Pipeline

Camera-only 3D perception attracts a large amount of attention from academia because it is an uncurated problem compared to LiDAR-based 3D perception and thus worth exploring. The core issue is that 2D images naturally do not preserve 3D information, hence it is difficult to obtain accurate 3D localization of objects when depth information is inaccurately extracted from 2D images. Camera-only 3D perception can be split into three domains: single-camera setting, stereo setting and multi-camera setting, and they have different skills to tackle down the depth problem. Since multi-camera methods often start with a single-camera baseline, we start with monocular (single-camera) baseline setting as well. We use “2D space” to refer to perspective view with camera plane coordinates, “3D space” to refer to 3D real-world space with world coordinates, and “BEV space” to refer to bird’s eye view in the following context.

As depicted in Fig. 2, a general monocular camera-only 3D perception system can be divided into three parts: 2D feature extractor, view transformation module (optional), and 3D decoder. As camera-only 3D perception has the same input as 2D perception, the general feature extractor can be formulated as

$$\mathcal{F}_{2D}^*(u, v) = M_{feat}(\mathcal{I}^*(u, v)), \quad (4)$$

where  $\mathcal{F}_{2D}$  denotes 2D feature,  $\mathcal{I}$  denotes image,  $M_{feat}$  denotes 2D feature extractor (usually as backbone network [79]

with FPN [80]),  $u, v$  denote coordinates on 2D plane and  $*$  denotes one or more images and corresponding 2D features. In 2D feature extractor, there exists a huge amount of experience in 2D perception that can be considered in 3D perception, in the form of backbone pretraining [79, 81]. The view transformation module largely differentiates from 2D perception system. Note that not all 3D perception methods have a view transformation module, and some detect objects in 3D space directly from features in 2D space [81, 82, 83]. As depicted in Fig. 2, there are generally two ways to perform view transformation, one is to perform transformation from 3D space to 2D space, the other is to conduct transformation from 2D space to 3D space, both of which is either using physical prior in 3D space or utilizing 3D supervision. Such a transformation can be formulated as:

$$\mathcal{F}_{3D}(x, y, z) = M_{trans}(\mathcal{F}_{2D}^*(\hat{u}, \hat{v}), [\mathbf{R} \ \mathbf{T}], \mathbf{K}), \quad (5)$$

where  $\mathcal{F}_{3D}$  denotes 3D (or voxel) feature,  $x, y, z$  denotes coordinate in 3D space,  $M_{trans}$  denotes view transformation module,  $\hat{u}, \hat{v}$  denotes corresponding 2D coordinates in terms of  $x, y, z$  (note that this may vary depending on the specific view transformation methods),  $[\mathbf{R} \ \mathbf{T}]$  and  $\mathbf{K}$  are camera extrinsics and intrinsics as defined in Sec. B.1 of Appendix. The 3D decoders receive the feature in 2D/3D space and output 3D perception results such as 3D bounding boxes, BEV map segmentation, 3D lane keypoints and so on. Most 3D decoders comes from LiDAR-based methods [44, 67, 84, 85] which are performing detection in voxel-space/BEV space, but still there are some camera-only 3D decoders that utilize the feature in 2D space [82, 83, 86] and directly regress the localization of 3D objects.

TABLE 3: Performance comparison of BEV perception algorithms on popular benchmarks. We classify different approaches following Tab. 2. Under **Modality**, “L” for LiDAR, “SC” for single camera, “MC” for multi camera. Under **Task Head**, “Det” for 3D object/lane detection task, “Seg” for BEV map segmentation task. Under **KITTI ODet**, we report  $AP_{40}$  of 3D object at Easy, Moderate and Hard level in KITTI dataset [11]. Under **nuS ODet**, we report **NDS** and  $mAP$  of 3D object in nuScenes dataset [7]. Under **nuS MapSeg**, we report mIOU score of DRI(drivable area) and LAN(lane, a.k.a divider) categories in nuScenes Map Segmentation setting. Under **OL**, we report F1 score of 3D laneline in OpenLane dataset [26]. Under **WOD**, we report LET-APL [61] for camera-only 3D object detection and APH/L2 [8] for any modality 3D object detection in Waymo Open Dataset [8]. \* denotes results reported by their papers with specific settings.

Methods	Modality			Task Head		KITTI ODet %			nuS ODet		nuS MapSeg		OL	WOD	
	SC	MC	L	Det	Seg	Easy	Mod.	Hard	NDS	mAP	DRI	LAN	F1	LET	APH/L2
OFT [43]	✓	-	-	✓	-	2.50	3.28	2.27	-	-	-	-	-	-	-
CaDDN [46]	✓	-	-	✓	-	19.17	13.41	11.46	-	-	-	-	-	-	-
ImVoxelNet [50]	✓	✓	-	✓	-	17.15	10.97	9.15	-	0.518*	-	-	-	-	-
DfM [10]	✓	-	-	✓	-	22.94	16.82	14.65	-	-	-	-	-	-	-
PGD [62]	✓	-	-	✓	-	19.05	11.76	9.39	0.448	0.386	-	-	-	0.5127	-
BEVerse [63]	-	✓	-	✓	-	-	-	-	0.531	0.393	-	-	-	-	-
PointPillars [45]	-	-	✓	✓	-	-	-	-	0.550	0.401	-	-	-	-	-
BEVDet [47]	-	✓	-	✓	-	-	-	-	0.552	0.422	-	-	-	-	-
BEVDet4D [64]	-	✓	-	✓	-	-	-	-	0.569	0.451	-	-	-	-	-
BEVDepth [49]	-	✓	-	✓	-	-	-	-	0.609	0.520	-	-	-	-	-
DSGN [65]	-	✓	-	✓	-	73.50	52.18	45.14	-	-	-	-	-	-	-
PV-RCNN [66]	-	-	✓	✓	-	-	-	-	-	-	-	-	-	-	0.7152
CenterPoint [67]	-	-	✓	✓	-	-	-	-	0.673	0.603	-	-	-	-	0.7193
SST [68]	-	-	✓	✓	-	-	-	-	-	-	-	-	-	-	0.7281
AFDetV2 [69]	-	-	✓	✓	-	-	-	-	0.685	0.624	-	-	-	-	0.7312
PV-RCNN++ [70]	-	-	✓	✓	-	-	-	-	-	-	-	-	-	-	0.7352
Pyramid-PV [71]	-	-	✓	✓	-	-	-	-	-	-	-	-	-	-	0.7443
MPPNet [72]	-	-	✓	✓	-	-	-	-	-	-	-	-	-	-	0.7567
M <sup>2</sup> BEV [3]	-	✓	-	✓	✓	-	-	-	0.474	0.429	77.3	40.5	-	-	-
BEVFormer [4]	-	✓	-	✓	✓	-	-	-	0.569	0.481	80.1	25.7	-	0.5616	-
PolarFormer [51]	-	✓	-	✓	✓	-	-	-	0.572	0.493	82.6	46.2	-	-	-
PointPainting [73]	-	✓	✓	✓	-	-	-	-	0.581	0.464	-	-	-	-	-
MVP [74]	-	✓	✓	✓	-	-	-	-	0.705	0.664	-	-	-	-	-
AutoAlign [75]	-	✓	✓	✓	-	-	-	-	0.709	0.658	-	-	-	-	-
TransFusion [76]	-	✓	✓	✓	-	-	-	-	0.717	0.689	-	-	-	-	-
DeepFusion [77]	-	✓	✓	✓	-	-	-	-	-	-	-	-	-	-	0.7554
AutoAlignV2 [78]	-	✓	✓	✓	-	-	-	-	0.724	0.684	-	-	-	-	-
BEVFusion [5]	-	✓	✓	✓	✓	-	-	-	0.761	0.750	85.5	53.7	-	-	0.7633
3D-LaneNet [59]	✓	-	-	✓	-	-	-	-	-	-	-	-	0.441	-	-
PersFormer [26]	✓	-	-	✓	-	-	-	-	-	-	-	-	0.505	-	-

As a side note, there are few attempt to solve 3D pre-training [81] and transfer recent success in 2D vision Transformer [87, 88] to 3D space; this could be future investigation in 3D perception.

### 3.1.2 View Transformation

Recent research has focused on view transformation module [3, 4, 10, 26, 47, 48, 49, 51, 56, 59], where 3D information is constructed from either 2D feature or 3D prior assumption. Constructing 3D information from 2D feature is usually formulated as depth estimation or cost volume. Constructing 3D information from 3D prior assumption is usually formulated as sampling 2D feature to construct 3D feature via 3D-2D projection mapping.

View transformation plays a vital role in camera-only 3D perception, as it is the main module that constructs 3D information and encode 3D prior assumption. By and large, it can be divided into two aspects, one is to utilize 2D feature to construct depth information and “lift” 2D feature to 3D

space, the other is to encode 2D feature to 3D space via 3D-to-2D projection mapping. We name the first method as 2D-3D and the second one 3D-2D. Fig. 3 presents a summary roadmap of performing view transformation via these two methods, and they are analyzed in details below.

The 2D-3D method is introduced by LSS [57], where it predicts depth distribution per grid on 2D feature, then “lift” the 2D feature per grid via the corresponding depth to voxel space, and perform downstream tasks following LiDAR-based methods. This process can be formulated as:

$$\mathcal{F}_{3D}(x, y, z) = [\mathcal{F}_{2D}^*(\hat{u}, \hat{v}) \otimes \mathcal{D}^*(\hat{u}, \hat{v})]_{xyz}, \quad (6)$$

where  $\mathcal{F}_{3D}(x, y, z)$  and  $\mathcal{F}_{2D}^*(\hat{u}, \hat{v})$  remain the same as Eqn. 5,  $\mathcal{D}^*(\hat{u}, \hat{v})$  represents predicted depth value or distribution at  $(\hat{u}, \hat{v})$ , and  $\otimes$  denotes outer production or similar operations. Note that this is very different from pseudo-LiDAR methods [89, 90] whose depth information is extracted from a pretrained depth estimation model and the lifting process

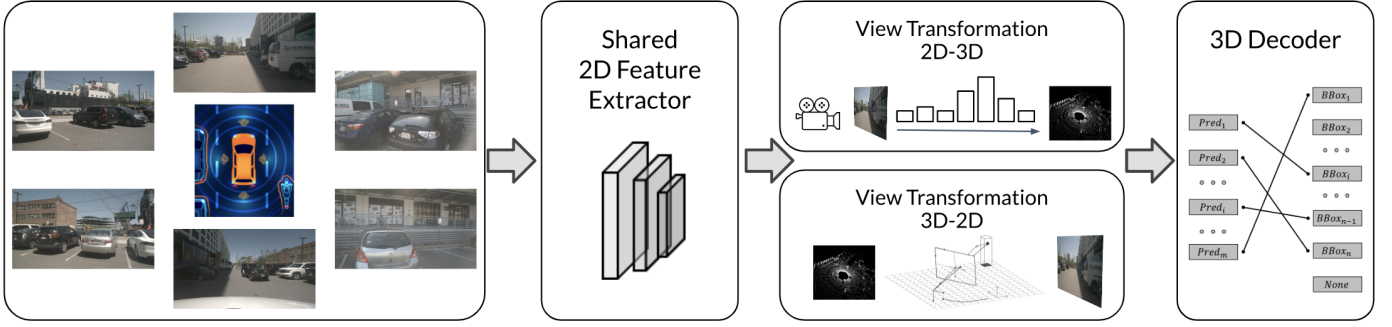


Fig. 2: The general pipeline of BEV Camera (camera-only perception). There are three parts, including 2D feature extractor, view transformation and 3D decoder. In view transformation, there are two ways to encode 3D information - one is to predict depth information from 2D feature; the other is to sample 2D feature from 3D space.

occurs before 2D feature extraction. After LSS [57], there is another work following the same idea of formulating depth as bin-wise distribution, namely CaDDN [46]. CaDDN employs a similar network to predict depth distribution (categorical depth distribution), squeezes the voxel-space feature down to BEV space, and performs 3D detection at the end. The main difference between LSS [57] and CaDDN [46] is that CaDDN uses depth ground truth to supervise its categorical depth distribution prediction, thus owing a superior depth network to extract 3D information from 2D space.

Note that when we claim “a better depth network”, it is actually learning an implicit projection between the road surface and the perspective view at feature level. This track comes subsequent work such as BEVDet [47] and its temporal version BEVDet4D [64], BEVDepth [49], BEVFusion [5, 91], and others [65, 81, 92]. Note that in stereo setting, depth value/distribution is much more easier to be obtained via the strong prior where the distance between the pair of cameras (namely *baseline* of the system) are supposed to be constant. This can be formulated as:

$$D(u, v) = f \times \frac{b}{d(u, v)}, \quad (7)$$

where  $d(u, v)$  is the horizontal disparity on the pair of images at location  $(u, v)$  (usually defined in the left image),  $f$  is the focal length of cameras as in Sec. B.1 of Appendix,  $D(u, v)$  is the depth value at  $(u, v)$ , and  $b$  is the length the baseline. Stereo methods such as LIGA Stereo [92] and DSGN [65] utilize this strong prior and perform on par with LiDAR-based alternatives on KITTI leaderboard [11].

The second branch (3D to 2D) can be originated back to thirty years ago, when Inverse Perspective Mapping (IPM) [93] formulated the projection from 3D space to 2D space conditionally hypothesizing that the corresponding points in 3D space lie on a horizontal plane. Such a transformation matrix can be mathematically derived from camera intrinsic and extrinsic parameters [94], and the detail of this process is presented in Sec. B.1 of Appendix. A series of work apply IPM to transform elements from perspective view to bird’s eye view in an either pre-processing or post-processing manner. In context of view transformation, the 3D-2D method, or feature projection from 3D to 2D, is first introduced by OFTNet [43], where it projects 2D feature to voxel space (3D space). It is based on assumption that the depth distribution is uniform along the ray starting from camera origin to a specific point in 3D space. Such

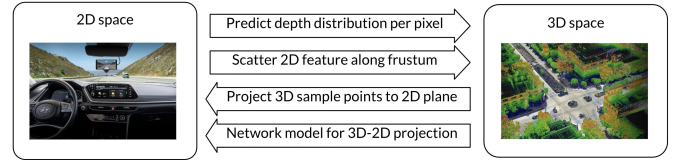


Fig. 3: View transformation taxonomy. From **2D to 3D**, LSS-based methods [5, 46, 47, 49, 57, 64, 91] predict depth distribution per pixel from 2D feature, while stereo methods [65, 92] scatter 2D feature along frustum constructed by cost volume. From **3D to 2D**, homographic-matrix-based methods [4, 26, 48, 56, 86, 96] presume sparse 3D sample points and project them to 2D plane via camera parameters. Pure-network-based methods use MLP or transformer to implicitly model the projection matrix from 3D space to 2D plane.

an assumption holds true for most scenes in autonomous driving, but sometimes breaks when it comes to undulating roads. Meanwhile, a lot of BEV map segmentation work [56] utilize either multi-layer perceptron or transformer architecture [95] to model the 3D-2D projection implicitly without camera parameters. Recently, a combination of 3D-2D geometric projection and neural network becomes popular [4, 26, 48, 56, 86, 96], inspired by Tesla releasing its technical roadmap for the perception system [6]. Note that the cross-attention mechanism in transformer architecture conceptually meets the need of such a geometric projection, as denoted by:

$$\mathcal{F}_{3D}(x, y, z) = \text{CrossAttn}(q : P_{xyz}, k, v : \mathcal{F}_{2D}^*(\hat{u}, \hat{v})), \quad (8)$$

where  $q, k, v$  stand for query, key and value,  $P_{xyz}$  is pre-defined anchor point in voxel space, and other notations follow Eqn. 4 and 5. Some approaches [4, 48, 86] utilize camera parameters to project  $P_{xyz}$  to image plane for fast convergence of the model. To obtain robust detection results, BEVFormer [4] exploits the cross-attention mechanism in transformer to enhance the modeling of 3D-2D view transformation. Others [50, 97] alleviate grid sampler to accelerate this process efficiently for massive production. However, these methods depend a lot on the accuracy of camera parameters, which are prone to change for a long period of driving.

### 3.1.3 Discussion on BEV and perspective methods

At the very beginning of camera-only 3D perception, the main focus is how to predict 3D object localization from perspective view, *a.k.a.* 2D space. It is because 2D perception is well developed at that stage [1, 2, 98, 99], and how to equip a 2D detector with the ability to perceive 3D scene becomes mainstream methods [62, 82, 83, 100]. Later, some research reached to BEV representation, since under this view, it is easy to tackle the problem where objects with the same size in 3D space have very different size on image plane due to the distance to camera. This series of work [43, 46, 65, 89, 92] either predict depth information or utilize 3D prior assumption to compensate the loss of 3D information in camera input. While recent BEV-based methods [3, 4, 5, 47, 49, 91, 101] has taken the 3D perception world by storm, it is worth noticing that this success has been beneficial from mainly three parts. The first reason is the trending nuScenes dataset [7], which has multi-camera setting and it is very suitable to apply multi-view feature aggregation under BEV. The second reason is that most camera-only BEV perception methods have gained a lot of help from LiDAR-based methods [44, 45, 67, 84, 85, 102, 103] in form of detection head and corresponding loss design. The third reason is that the long-term development of monocular methods [82, 83, 100] has flourished BEV-based methods a good starting point in form of handling feature representation in the perspective view. The core issue is how to reconstruct the lost 3D information from 2D images. To this end, BEV-based methods and perspective methods are two different ways to resolve the same problem, and they are not excluding each other.

## 3.2 BEV LiDAR

### 3.2.1 General Pipeline

Fig. 4 depicts the general pipeline for BEV LiDAR perception. The extracted point cloud features are transformed into BEV feature maps. The common detection heads generate 3D prediction results. In terms of the feature extraction part, there are mainly two branches to convert point cloud data into BEV representation. According to the pipeline order, we term these two options as pre-BEV and post-BEV respectively, indicating whether the input of backbone network is from 3D representation or BEV representation.

### 3.2.2 Pre-BEV Feature Extraction

Besides point-based methods processing on the raw point cloud, voxel-based methods voxelize points into discrete grids, which provides a more efficient representation by discretizing the continuous 3D coordinate. Based on the discrete voxel representation, 3D convolution or 3D sparse convolution [116, 117] can be used to extract point cloud features. We use  $Y_{j,c'}$  to represent the  $j$ -th voxel output  $Y$  at output channel  $c'$ , and  $X_{i,c}$  to represent the  $i$ -th voxel input  $X$  at input channel  $c$ . A normal 3D convolutional operation can be described as:

$$Y_{j,c'} = \sum_{i \in P(j)} \sum_c W_{k,c,c'} X_{i,c}, \quad (9)$$

where  $P(j)$  denotes a function for obtaining the input index  $i$  and the filter offset, and  $W_{k,c,c'}$  denotes filter weight with

kernel offset  $k$ . For sparse input  $\tilde{X}$  and output  $\tilde{Y}$ , we can rewrite Eqn. 9 into 3D sparse convolution:

$$\tilde{Y}_{j,c'} = \sum_k \sum_c W_{k,c,c'} \tilde{X}_{R_{k,j},k,c}, \quad (10)$$

where  $R_{k,j}$  denotes a matrix that specifies the input index  $i$  given the kernel offset  $k$  and the output index  $j$ . Most state-of-the-art methods normally utilize 3D sparse convolution to conduct feature extraction. The 3D voxel features can then be formatted as a 2D tensor in BEV by densifying and compressing the height axis.

VoxelNet [44] stacks multiple voxel feature encoding (VFE) layers to encode point cloud distribution in a voxel as a voxel feature. Given  $\mathbf{V} = \{\mathbf{p}_i = [x_i, y_i, z_i, r_i]^T\}_{i=1 \dots n}$  as  $n \leq N$  points inside a non-empty voxel, where  $x_i, y_i, z_i$  are coordinates in 3D space,  $r_i$  is reflectance,  $N$  is the maximal number of points, and the centroid of  $\mathbf{V}$  ( $v_x, v_y, v_z$ ) is the local mean of all points, the feature of each point is calculated by:

$$f_i = FCN([x_i, y_i, z_i, r_i, x_i - v_x, y_i - v_y, z_i - v_z]^T). \quad (11)$$

FCN is the composition of a linear layer, a batch normalization, and an activation function. Feature of the voxel is the element-wise max-pooling of all  $f_i$  of  $\mathbf{V}$ . A 3D convolution is applied to further aggregate local voxel features. After merging the dimension of channel and height, the feature maps, which are transformed implicitly into BEV, are processed by a region proposal network (RPN) to generate object proposals. SECOND [85] introduces sparse convolution in processing voxel representation to reduce training and inference speed by a large margin. CenterPoint [67], which is a powerful center-based anchor-free 3D detector, also follows this detection pattern and becomes a baseline method for 3D object detection.

PV-RCNN [66] combines point and voxel branches to learn more discriminative point cloud features. Specifically, high-quality 3D proposals are generated by the voxel branch, and the point branch provides extra information for proposal refinement. SA-SSD [104] designs an auxiliary network, which converts the voxel features in the backbone network back to point-level representations, to explicitly leverage the structure information of the 3D point cloud and ease the loss in downsampling. Voxel R-CNN [106] adopts 3D convolution backbone to extract point cloud feature. A 2D network is then applied on the BEV to provide object proposals, which are refined via extracted features. It achieves comparable performance with point-based methods. Object DGCNN [107] models the task of 3D object detection as message passing on a dynamic graph in BEV. After transforming point cloud into BEV feature maps, predicted query points collect BEV features from key points iteratively. VoTr [105] introduces Local Attention, Dilated Attention, and Fast Voxel Query to enable attention mechanism on numerous voxels for large context information. SST [68] treats extracted voxel features as tokens and then applies Sparse Regional Attention and Region Shift in the non-overlapping region to avoid downsampling for voxel-based networks. AFDetV2 [69] formulates a single-stage anchor-free network by introducing a keypoint auxiliary supervision and multi-task head.

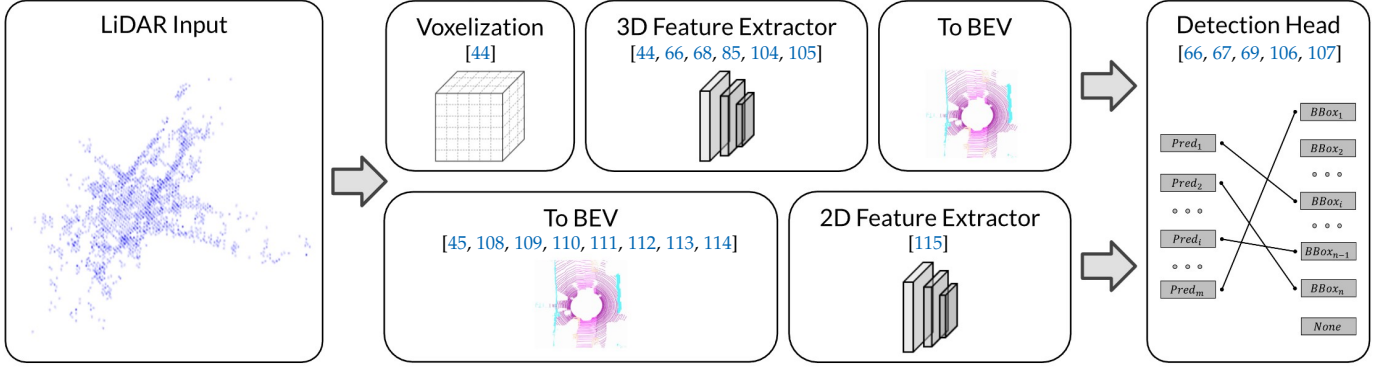


Fig. 4: The general pipeline of BEV LiDAR perception. There are mainly two branches to convert point cloud data into BEV representation. The upper branch extracts point cloud features in 3D space, providing more accurate detection results. The lower branch extracts BEV features in 2D space, providing more efficient networks.

### 3.2.3 Post-BEV Feature Extraction

As voxels in 3D space are sparse and irregular, applying 3D convolution is inefficient. For industrial applications, operators such as 3D convolution may not be supported; suitable and efficient 3D detection networks are desirable.

MV3D [108] is the first method to convert point cloud data into a BEV representation. After discretizing points into the BEV grid, the features of height, intensity, and density are obtained according to points in the grid to represent grid features. As there are many points in a BEV grid, in this processing, the loss of information is considerable. Other works [109, 110, 111, 112, 113, 114] follow the similar pattern to represent point cloud using the statistic in a BEV grid, such as the maximum height and mean of intensity.

PointPillars [45] first introduces the concept of pillar, which is a special type of voxel with unlimited height. It utilizes a simplified version of PointNet [102] to learn a representation of points in pillars. The encoded features can then be processed by standard 2D convolutional networks and detection heads. Though the performance of PointPillars is not as satisfactory as other 3D backbones, it and its variants enjoy high efficiency and thus are suitable for industrial applications.

### 3.2.4 Discussion

The point cloud data are directly processed by the neural network, as does in [118, 119]. The neighborhood relationship among points is calculated in the continuous 3D space. This brings extra time consumption and limits the receptive field of the neural network. Recent work [44, 85] utilize discrete grids to represent point cloud data; convolutional operations are adopted to extract features. However, converting point cloud data into any form of representation inevitably causes the loss of information. State-of-the-art methods in pre-BEV feature extraction utilize voxels with fine-grained size, preserving most of the 3D information from point cloud data and thus beneficial for 3D detection. As a trade-off, it requires high memory consumption and computational cost. Transforming point cloud data directly into BEV representation avoids complex operation in the 3D space. As the height dimension is compressed, a great loss of information becomes inevitable. The most efficient method is to represent the BEV feature map using statistics, and yet it provides inferior results. Pillar-based methods [45]

balance performance and cost, and become a popular choice for industrial applications. How to deal with the trade-off between performance and efficiency becomes a vital challenge for LiDAR-based applications.

## 3.3 BEV Fusion

### 3.3.1 General Pipeline

Inverse perspective mapping (IPM) [120] is proposed to map pixels onto the BEV plane using the geometric constraint of the intrinsic and extrinsic matrix of cameras. Despite its inaccuracy due to the flat-ground assumption, it provides the possibility that images and point clouds can be unified in BEV. Lift-splat-shoot (LSS) [57] is the first method to predict depth distribution of image features, introducing neural networks to learn the ill-posed camera-to-lidar transformation problem. Other works [4, 121] develop different method to conduct view transformation. Given the view transformation methods from perspective view to BEV, Fig. 5b shows the general pipeline for fusing image and point cloud data. Modal-specific feature extractors are used to extract features in perspective view and BEV separately. After transforming to the representations in BEV, feature maps from different sensors are fused. The temporal and ego-motion information can be introduced in the BEV representation as well.

### 3.3.2 LiDAR-camera Fusion

Concurrently, two works with the same name BEVFusion [5, 91] explore fusion in BEV from different directions. As camera-to-lidar projection [73, 122] throws away the semantic density of camera features, BEVFusion [5] designs an efficient camera-to-BEV transformation method, which efficiently projects camera features into BEV, and then fuses it with lidar BEV features using convolutional layers. BEVFusion [91] regards the BEV fusion as a robustness topic to maintain the stability of the perception system. It encodes camera and lidar features into the same BEV to ensure the independence of camera and lidar streams. This design enables the perception system to maintain stability against sensor failures.

Apart from BEVFusion [5, 91], UVTR [121] represents different input modalities in modal-specific voxel spaces without height compression to avoid the semantic ambiguity and enable further interactions. Image voxel space is

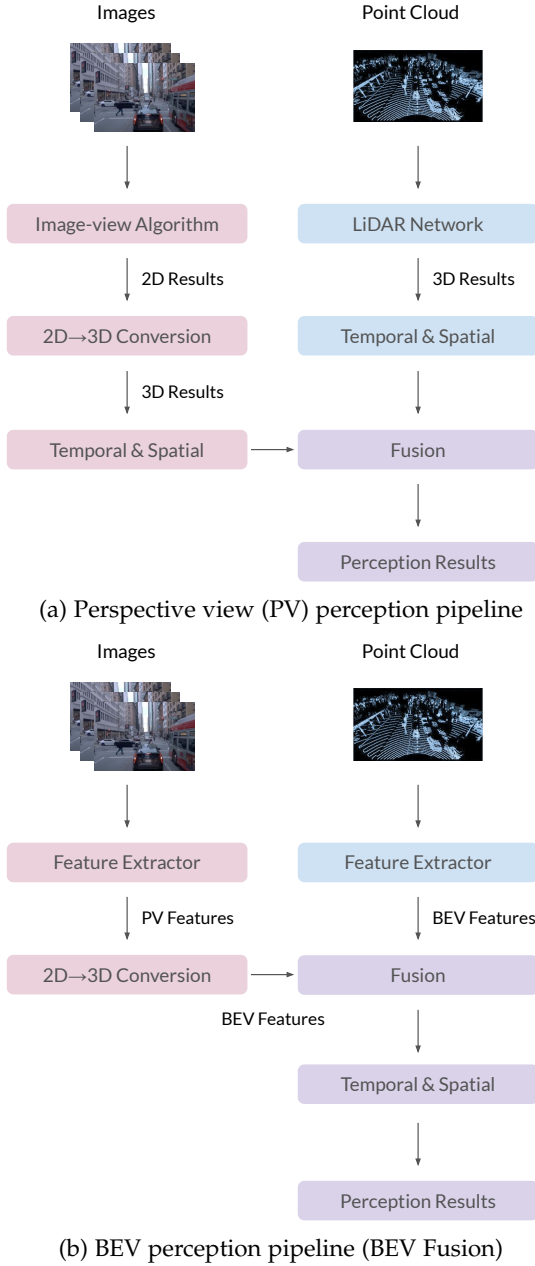


Fig. 5: Two typical pipeline designs for BEV fusion algorithms, applicable to both academia and industry. The main difference lies in 2D to 3D conversion and fusion modules. In the PV perception pipeline (a), results of different algorithm are first transformed into 3D space, then fused using prior or hand-craft rules. The BEV perception pipeline (b) first transforms PV features to BEV, then fuses features to obtain the ultimate predictions, thereby maintaining most original information and avoiding hand-crafted design.

constructed by transforming the image feature of each view to the predefined space with depth distribution generated for each image. Point voxel space is constructed using common 3D convolutional networks. Cross-modality interaction is then conducted between two voxel spaces to enhance modal-specific information.

### 3.3.3 Temporal Fusion

Temporal information plays an important role in inferring the motion state of objects and recognizing occlusions. BEV provides a desirable bridge to connect scene representations in different timestamps, as the central location of the BEV feature map is persistent to ego car. MVFuseNet [123] utilizes both BEV and range view for temporal feature extraction. Other works [53, 63, 64] use ego-motion to align the previous BEV features to the current coordinates, and then fuse the current BEV features to obtain the temporal features. BEVDet4D [64] fuses the previous feature maps with the current frame using a spatial alignment operation followed by a concatenation of multiple feature maps. BEVFormer [4] and UniFormer [124] adopt a soft way to fusion temporal information. The attention module is utilized to fuse temporal information from previous BEV feature maps and previous frames, respectively. Concerning the motion of ego car, locations for the attention module to attend among representations of different timestamps are also corrected by the ego-motion information.

### 3.3.4 Discussion

As images are in perspective coordinate and point clouds are in 3D coordinate, spacial alignment between two modalities becomes a vital problem. Though it is easy to project point cloud data onto image coordinates using geometric projection relationships, the sparse nature of point cloud data makes extracting informative features difficult. Inversely, transforming images in perspective view into 3D space would be an ill-posed problem, due to the lack of depth information in perspective view. Based on prior knowledge, previous work such as IPM [120] and LSS [57] make it possible to transform information in the perspective view into BEV, providing a unified representation for multi-sensor and temporal fusion.

Fusion in the BEV space for lidar and camera data provides satisfactory performance for the 3D detection task. Such a method also maintains the independence of different modalities, which provides the opportunity to build a more robust perception system. For temporal fusion, representations in different timestamps can be directly fused in the BEV space by concerning ego-motion information. Compensation for ego-motion is easy to obtain by monitoring control and motion information, as the BEV coordinate is consistent with the 3D coordinate. With the concern of robustness and consistency, BEV is an ideal representation for multi-sensor and temporal fusion.

## 3.4 Industrial Design of BEV Perception

Recent years have witnessed trending popularity for BEV perception in the industry. In this section, we describe the architecture design for BEV perception on a system level.

Fig. 5 depicts two typical paradigms for sensor fusion in the industrial applications. Prior to BEV perception research, most autonomous driving companies construct the perception system based on perspective view inputs. As shown in Fig. 5a, for the perspective view (PV) pipeline, LiDAR track generates 3D results directly. The 3D results from images are transformed from 2D results, based on geometry prior. Then we fuse the prediction from images and LiDAR, utilizing

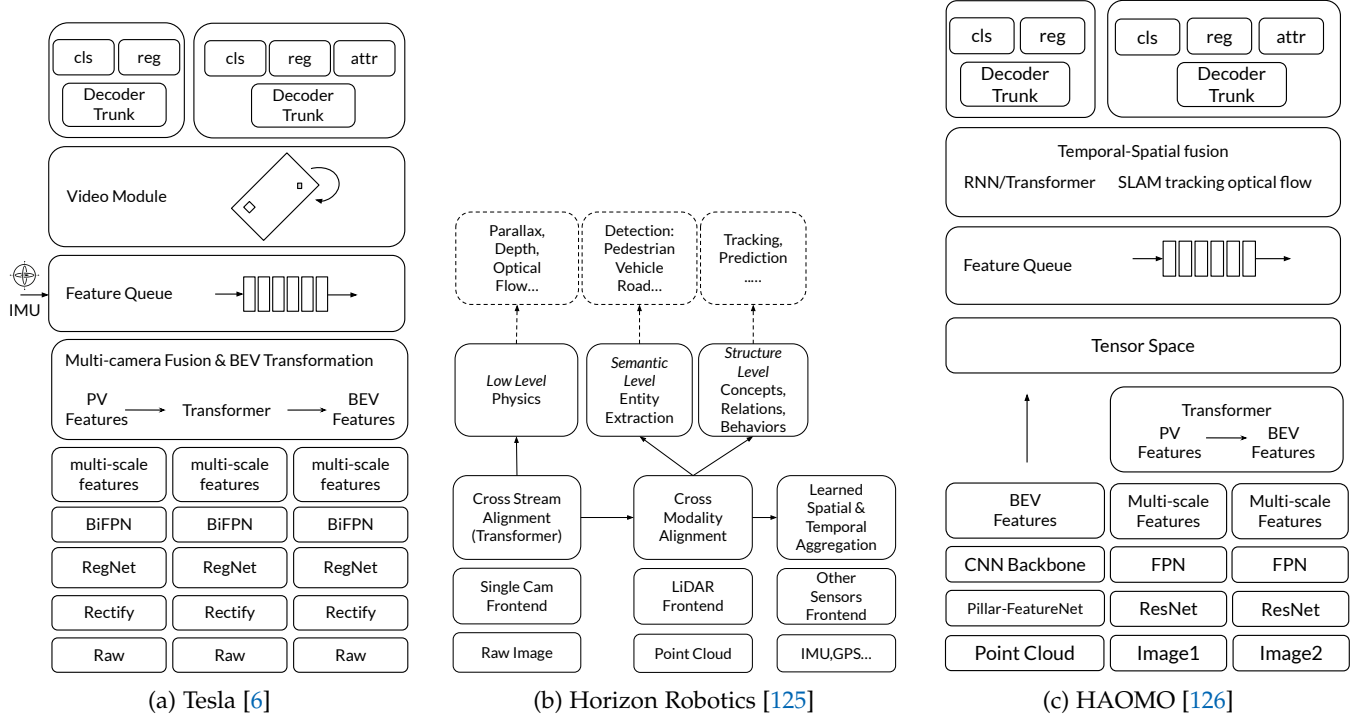


Fig. 6: BEV architecture comparison across industrial corporations. These paradigms follow similar workflow as illustrated in Fig. 5b unanimously (input sensors might vary). First they encode input data with backbone and perform BEV projection via transformer. Then, BEV features are fused temporally and spatially. At last, they decode BEV feature with different heads. There are slight differences in each design. Tesla takes camera image and IMU as input while Horizon and HAOMO embrace point clouds to the inputs additionally. Backbone varies in different architectures.

some hand-crafted approaches which do not always perform well on realistic scenarios. On the contrary, BEV based methods, as illustrated in Fig. 5b, perform 2D to 3D transformation with neural networks and integrate features instead of the direct detection outputs from different modalities, leading to less hand-crafted design and more robustness.

Fig. 6 summarizes various BEV perception architecture proposed by corporations around the globe. The detailed model/input options are described in Sec. D of Appendix. Note that all the information presented in this survey are collected from public resource; comparison and analysis among different plans are based on facts. **We do NOT advocate, oppose or advertise some plan towards other alternatives.** The BEV fusion architectures in Fig. 6 follow the pipeline as depicted in Fig. 5b, consisting of input data, feature extractor, PV to BEV transformation, feature fusion module, temporal & spatial module and prediction head. We elaborate on each module in details below.

### 3.4.1 Input Data

BEV based perception algorithms support different data modalities, including camera, LiDAR, Radar, IMU and GPS. Camera and LiDAR are the main perception sensors for autonomous driving. Some products use camera only as the input sensor, e.g., Tesla [6], PhiGent [127], Mobileye [128]. The others adopt a suite of camera and LiDAR combination, e.g., Horizon [125], HAOMO [126]. Note that IMU and GPS signals are often adopted for sensor fusion plans [6, 125, 126], as do in Tesla and Horizon, etc.

### 3.4.2 Feature Extractor

The feature extractor serves as transforming raw data to appropriate feature representations, and this module often consists of backbone and neck. There are different combinations for the feature extractor as backbone and neck. For instance, ResNet [115] in HAOMO [126] and RegNet [129] in Tesla [6] can be employed as the image backbone. The neck could be FPN [80] from HAOMO [126], BiFPN [130] as in Tesla [6], etc. As for the point cloud input, pillar based option from HAOMO [126] or voxel based choice from Mobileye are ideal candidates for the backbone.

### 3.4.3 PV to BEV Transformation

There are mainly four approaches to perform view transformation in industry: (a) **Fixed IPM**. Based on the flat ground assumption, a fixed transformation can project PV feature to BEV space. Fixed IPM projection handles ground plane well. However, it is sensitive to vehicle jolting and road flatness. (b) **Adaptive IPM** utilizes the extrinsic parameters of SDV, which are obtained by some pose estimation approaches, and projects features to BEV accordingly. Although adaptive IPM is robust to vehicle pose, it still hypothesizes on the flat ground assumption. (c) **Transformer** based BEV transformation employs dense transformer to project PV feature into BEV space. This data driven transformation operates well without prior assumption, and are thereby widely adopted by Tesla, Horizon, HAOMO. (d) **ViDAR** is first proposed in early 2018 by Waymo and Mobileye in parallel at different venues [13, 128], to indicate the practice of using pixel-level depth to project PV feature to BEV space based on camera or vision inputs, resembling the representation

form as does in LiDAR. The term ViDAR is equivalent to the concept of pseudo-LiDAR presented in most academic literature. Equipped With ViDAR, one can transform images and subsequently features into point cloud directly. Then point cloud based methods can be applied to get BEV features. We have seen many ViDAR applications recently, e.g., Tesla, Mobileye, Waymo, Toyota, [6, 13, 128, 131, 132], etc. Overall, the options of Transformer and ViDAR are most prevailing in industry.

#### 3.4.4 Fusion Module

The alignment among different camera sources has been accomplished in the previous BEV transformation module. In the fusion unit, they step further to aggregate BEV features from camera and LiDAR. By doing so, features from different modalities are ultimately integrated into one unified form.

#### 3.4.5 Temporal & Spatial Module

By stacking BEV features temporally and spatially, one can construct a feature queue. The temporal stack pushes and pops a feature blob every fixed time, while the spatial stack does it every fixed distance. After fusing feature in these stacks into one form, they can obtain a spatial-temporal BEV feature, which is robust to occlusion [6, 126]. The aggregation module can be in form of 3D convolution, RNN or Transformer. Based on the temporal module and vehicle kinematics, one can maintain a large BEV feature map surrounding ego vehicle and update the feature map locally, as does in the spatial RNN module from Tesla [6].

#### 3.4.6 Prediction Head

In BEV perception, the multi-head design is widely adopted. Since BEV feature aggregates information from all sensors, all 3D detection results are decoded from BEV feature space. In the meanwhile, PV results (which are still valuable for autonomous driving) are also decoded from the corresponding PV features in some design. The prediction results can be classified into three categories [125]: (a) **Low level results** are related to physics constrains, such as optical flow, depth, etc. (b) **Entity level results** include concepts of objects, i.e., vehicle detection, laneline detection, etc. (c) **Structure level results** represent relationship between objects, including object tracking, motion prediction, etc.

## 4 EMPIRICAL EVALUATION AND RECIPE

In this section, we summarize bag of tricks and most useful practice to achieve top results on various benchmarks. This is based on our contest entries to Waymo Open Challenge 2022, namely BEVFormer++ built on top of BEVFormer [4] for camera-only detection and Voxel-SPVCNN derived from SPVCNN [84] for LiDAR segmentation.

### 4.1 Data Augmentation

#### 4.1.1 BEV Camera (Camera-only) Detection

Common data augmentations on images for 2D recognition tasks are applicable for the tasks of camera based BEV perception. In general, we can divide augmentations into static augmentation involving color variation alone and

spatial transformation moving pixels around. Augmentations based on color variation are directly applicable. For augmentations involving spatial transformation, apart from ground truth transformed accordingly, calibration in camera parameter is also necessary. Common augmentations adopted in recent work are color jitter, flip, multi-scale resize, rotation, crop and grid mask.

In BEVFormer++, color jitter, flip, multi-scale resize and grid mask are employed. The input image is scaled by a factor between 0.5 and 1.2, flipped by a ratio of 0.5; the maximum 30% of total area is randomly masked with square masks. Notably, there two ways for flipping images in BEV perception. The first way is to simply flip image, ground truth and camera parameters accordingly. The second way also flips image orders to maintain coherence in overlapped area between images, which resembles to flip the whole 3D space symmetrically. The second way of flip is adopted in BEVFormer++. Related ablation study is described in Tab. 4 ID 6 experiment, indicating that data augmentation plays a vital role in improving 3D model's performance. Since BEVFormer [4] employs sequence input, it ensures that the transformation is consistent for each frame of the sequence after input augmentation.

#### 4.1.2 LiDAR Segmentation

Different from the task of detection, heavy data augmentation can be applied in the task of segmentation, including random rotation, scaling, flipping, and point translation. For random rotation, an angle is picked from the range of  $[0, 2\pi)$ , rotation is applied to every point on the  $x-y$  plane. A scale factor is chosen from the range of  $[0.9, 1.1]$ , and then multiplied on the point cloud coordinate. Random flipping is conducted along  $X$  axis,  $Y$  axis, or both  $X$  and  $Y$  axes. For random translation, offsets for each axis are sampled separately from a normal distribution with a mean of 0 and a standard deviation of 0.1.

Besides coordinates and reflectance, extra information can be utilized to boost model performance. Painting [73, 122] is a common technique to enhance point cloud data with image information. For unlabeled image data, by projecting point cloud labels onto corresponding images and densifying the sparse annotations, semantic labels on images are obtained from annotated point cloud data. An image model is trained to provide 2D semantic segmentation results. Then, predicted semantic labels are painted as one-hot vectors to point cloud data as additional channels to represent semantic information from images. Besides, temporal information can also be used, as datasets in autonomous driving are usually collected sequentially. Past consecutive frames are concatenated with the current frame. An additional channel is appended to represent the relative time information of different frames. To reduce the number of points, a small voxelization network is applied. Then, voxels treated as points are served as input to our models.

As shown in Tab. 5 ID 1, heavy data augmentation brings an improvement of mIoU of 0.4. By introducing information from images and previous frames, gains in model performance are 0.5 and 0.8 mIoU, respectively (Tab. 5 ID 5 & 6). It indicates that extra information, especially temporal information, is beneficial for the per-point classification task.

TABLE 4: **BEV camera detection track.** Ablation studies on `val` set with improvements over BEVFormer [4], i.e., BEVFormer++. Some results are only reported as  $L1/mAPH$  on *car* category with  $iou \geq 0.5$ . DeD (Deformable DETR head). FrA (FreeAnchor head). CeP (Centerpoint head). ConvO (Conv offsets in TSA). DE (Deformable view Encoder). CoP (Corner Pooling). DA (2D Auxiliary loss). GR (Global location regression). MS (Multi-Scale), FL (filp), SL (Smooth L1 Loss), EMA (Exponential Moving Average), SB (Sync BN), 2BS (2x BEV Scale), LLW (Learnable Loss Weight), LS (Label Smoothing), LE (LET-IoU based Assignment) and TTA (Test Time Augmentation). DS (Dataset). The `mini` dataset contains  $1/5$  training data. \*denotes the model is trained with 24 epochs, otherwise with 12 epochs.

ID	DeD	FrA	CeP	ConvO	DE	CoP	DA	GR	MS	FL	SL	EMA	SB	2BS	LLW	LS	LE	TTA	Backbone	DS	LET-mAPL	LET-mAPH	L1/mAPH
0	✓																		R101	mini	34.6	46.1	25.5
1	✓			✓															R101	mini	35.9	48.1	25.6
2	✓				✓														R101	mini	36.1	48.1	25.9
3	✓					✓													R101	mini	35.6	46.9	26.0
4	✓						✓									✓			R101	mini	36.2	48.1	25.4
5	✓							✓											R101	mini	35.4	47.2	27.2
6	✓								✓	✓									R101	mini	-	-	26.8
7	✓									✓	✓								R101	mini	-	-	27.3
8	✓											✓							R101	mini	-	-	26.2
9	✓												✓						R101	mini	-	-	25.6
9	✓													✓					R101	mini	-	-	25.5
10	✓														✓				R101	mini	-	-	26.5
11	✓															✓			R101	mini	36.0	46.7	-
12	✓																✓		R101	mini	34.7	44.2	-
13	✓			✓	✓	✓	✓	✓	✓	✓	✓	✓	✓	✓				✓	R101	mini	-	-	37.5
14*	✓			✓	✓	✓	✓	✓	✓	✓	✓	✓	✓	✓					SwinL	mini	40.0	55.6	51.9
15*	✓			✓	✓	✓	✓	✓	✓	✓	✓	✓	✓	✓					SwinL	mini	44.7	60.8	55.5
16		✓																	R101	mini	35.9	49.9	45.9
17		✓															✓		R101	mini	36.3	51.1	46.6
18			✓																R101	mini	34.0	47.9	43.5
19	✓			✓	✓	✓	✓	✓	✓	✓	✓	✓	✓	✓					SwinL	full	48.4	64.8	60.4
20		✓		✓	✓	✓	✓	✓	✓	✓	✓	✓	✓	✓					SwinL	full	47.2	61.2	56.8
21		✓		✓	✓	✓	✓	✓	✓	✓	✓	✓	✓	✓			✓		SwinL	full	47.6	61.4	57.0
22			✓	✓	✓	✓	✓	✓	✓	✓	✓	✓	✓	✓					SwinL	full	41.9	54.6	48.2

TABLE 5: **BEV LiDAR segmentation track.** Ablation studies on `val` set with improvements over SPVCNN [84], i.e., Voxel-SPVCNN. Aug (heavy data augmentation). Arch (adjustments on model architecture). TTA (test-time augmentation). Painting (one-hot painting from image semantic segmentation). Temporal (multi-frame input). V-SPV (Voxel-SPVCNN). Expert (ensemble with more expert models). Post (post-processing techniques including object-level refinement and segmentation with tracking).

ID	Aug	Loss	Arch	TTA	Painting	Temporal	V-SPV	Ensemble	Expert	Post	mIoU
0											67.4
1	✓										67.8
2	✓	✓									68.4
3	✓	✓	✓								69.6
4	✓	✓	✓	✓							71.1
5	✓	✓	✓	✓	✓						71.6
6	✓	✓	✓	✓	✓	✓					72.4
7	✓	✓	✓	✓	✓	✓	✓				73.5
8	✓	✓	✓	✓	✓	✓	✓	✓			74.2
9	✓	✓	✓	✓	✓	✓	✓	✓	✓		74.5
10	✓	✓	✓	✓	✓	✓	✓	✓	✓	✓	75.4

## 4.2 BEV Encoder

### 4.2.1 BEV Camera: BEVFormer++

BEVFormer++ has multiple encoder layers, each of which follows the conventional structure of transformers [95], except for three tailored designs, namely BEV queries, spatial cross-attention, and temporal self-attention. Specifically, BEV queries are grid-shaped learnable parameters, which is designed to query features in BEV space from multi-camera views via attention mechanisms. Spatial cross-attention and temporal self-attention are attention layers working with BEV queries, which are used to lookup and aggregate spatial features from multi-camera images as well as temporal features from history BEV, according to the BEV query.

During inference, at timestamp  $t$ , we feed multi-camera

images to the backbone network (e.g., ResNet-101 [115]), and obtain the features  $F_t = \{F_t^i\}_{i=1}^{N_{view}}$  of different camera views, where  $F_t^i$  is the feature of the  $i$ -th view,  $N_{view}$  is the total number of camera views. At the same time, we preserve BEV features  $B_{t-1}$  at the prior timestamp  $t-1$ . In each encoder layer, we first use BEV queries  $Q$  to query the temporal information from the prior BEV features  $B_{t-1}$  via the temporal self-attention. We then employ BEV queries  $Q$  to inquire about the spatial information from multi-camera features  $F_t$  via the spatial cross-attention. After the feed-forward network [95], the encoder layer generates the refined BEV features, which is consequently the input of the next encoder layer. After six stacking encoder layers, unified BEV features  $B_t$  at current timestamp  $t$  are generated.

Taking the BEV features  $B_t$  as input, the 3D detection head and map segmentation head predict the perception results such as 3D bounding boxes and semantic map.

To improve the feature quality contributing from BEV encoder, three main aspects are to be discussed as follows.

**(a) 2D Feature Extractor.** Techniques for improving backbone representation quality in 2D perception tasks are most likely to improve presentation quality for BEV tasks as well. For convenience, in the image backbone we adopt feature pyramid that is widely used in most 2D perception tasks. As depicted in Tab. 4, the structural design of 2D feature extractor, e.g. state-of-the-art image feature extractor [133], global information interaction [134], multi-level feature fusion [80, 135] etc. all contribute to better feature representation for BEV perception. Apart from the structural design, auxiliary tasks supervising backbones are also important for the performance of BEV perception, which will be discussed in Sec. 4.5.1.

**(b) View transformation.** The transformation takes in image features and reorganizes them into BEV space. Hyper-parameters, including the image feature’s sampling range and frequency, as well as BEV resolution are of vital importance for the performance of BEV perception. The sampling range decides how much of the viewing frustum behind an image will be sampled into BEV space. By default this range is equal to the effective range of LiDAR annotation. When efficiency is of higher priority, the upper z-axis part of the viewing frustum can be compromised since it only contains unimportant information such as sky in most cases. The sampling frequency decides the utility of image features. Higher frequency ensures the model to accurately sample corresponding image features for each BEV location with the cost of higher computation. BEV resolution decides the representation granularity of the BEV feature, where each feature can be accurately traced back to a grid in the world coordinates. High resolution is required for better representation of small scale objects such as traffic lights and pedestrians. Related experiments are depicted in Tab. 4 ID 2&3. In view transformation, feature extraction operations, e.g. convolution block or Transformer block are also present in many BEV perception networks. Adding better feature extraction sub-networks in the BEV space can also improve the BEV perception performance.

**(c) Temporal BEV fusion.** Given the structure of BEV feature, temporal fusion in BEV space often leverages ego-car pose information to align temporal BEV features. However, other agents’ movements are not modeled explicitly in this alignment process and it requires additional learning by the model. As a result, to enhance fusion on features of other moving agents, it is reasonable to increase the perception range of cross-attention as we perform temporal fusion. For instance, we might enlarge the kernel size of attention offset in the deformable attention module or use global attention. Related improvements can be observed in Tab. 4 ID 1.

#### 4.2.2 BEV LiDAR: Voxel-SPVCNN

Existing 3D perception models are not ideal to recognize small instances due to the coarse voxelization and aggressive downsampling. SPVCNN [84] utilizes Minkowski U-Net [117] in the voxel-based branch. To preserve point cloud

resolution, an extra point-based branch without downsampling is used. Features of the point-based and voxel-based branches would be propagated to each other at different stages of the network.

We propose Voxel-SPVCNN by making two effective modifications to the original SPVCNN [84]. Compared to simply performing voxelization on the raw input feature, a lightweight 3-layer MLP is applied to extract point features and then the voxelization process is applied. Besides, the input of the point-based branch is replaced by the voxel-as-point branch. The network structure of this branch is still a MLP; but the input is replaced as voxels. Voxel-SPVCNN is more efficient, as computation on the point-based branch is greatly reduced, especially in the case where the input is multi-scan point cloud. The change of model architecture brings an improvement of 1.1 mIoU (see Tab. 5 ID 7).

### 4.3 3D Detection Head in BEVFormer++

We mainly refer to BEV camera detection task for this trick. In BEVFormer++, three detection heads are adopted. Correspondingly, these heads cover three categories of the detector design, including anchor-free, anchor-based and center-based. We choose various types of detector heads that differentiate in design as much as possible, so as to fully leverage detection frameworks for the potential ability in different scenarios. The diversity of heads facilitate the ultimate ensemble results.

Original BEVFormer uses a modified Deformable DETR decoder as its 3D detector [4, 135, 136], which can detect 3D bounding boxes end-to-end without NMS. For this head, we follow the original design but use Smooth L1 loss to replace the origin L1 loss. Most of our baseline experiments with tricks are implemented on the DETR decoder, as described in Tab. 4 ID 1-15.

BEVFormer++ adopts the FreeAnchor [137] and CenterPoint [67] as alternative 3D detectors, where FreeAnchor is an anchor-based detector that can automatically learns the matching of anchors, and CenterPoint being a center-based anchor-free 3D detector. Ablation study in Tab. 4 ID 16-20 indicates that these heads perform differently under various settings. This is important for the ensemble part since prediction heads provide various distribution during inference. More details about the ensemble technique can be found in Sec. 4.6.1. It is worth noting that 3D decoder is far from being well developed, as efficient query design [87, 88] gets it prosperity in 2D perception. How to transfer those success to 3D perception field would be the next step in this community.

### 4.4 Test-time Augmentation (TTA)

#### 4.4.1 BEV Camera-only Detection

Common test-time augmentation for 2D tasks, including multi-scale and flip testing are examined to improve accuracy in 3D case as well. In BEVFormer++, this part is simply explored in form of utilizing standard data augmentation such as multi-scale and flip. The extent of multi-scale augmentation are the same as training, varying from 0.75 to 1.25. Related experiments are shown in Tab. 4 ID 13.

#### 4.4.2 LiDAR Segmentation

During inference, multiple TTAs are utilized, including rotation, scaling, and flipping. For scaling, the scaling factor is set to  $\{0.90, 0.95, 1.00, 1.05, 1.10\}$  for all models, since a larger or smaller scaling factor is harmful to model performance. Flipping remains the same as in the training phase, namely, along  $X$  axis,  $Y$  axis, and both  $X$  and  $Y$  axes. Rotation angle is set to  $\{-\frac{\pi}{2}, 0, \frac{\pi}{2}, \pi\}$ . A more fine-grained scaling factor or rotation angle could be chosen, but with the concern of computation overhead and the strategy of TTA combination, coarse-grained parameters are preferable.

A combination of TTAs would further improve model performance, compared to fine-grained augmentation parameters. However, it is time-consuming due to the multiplication of TTAs. The combined model-dependent TTAs with 20 inference time is employed. Grid search of combination strategy could be conducted. Empirically, a combination of scaling and flipping is preferable. An obvious improvement of 1.5 mIoU can be obtained (see Tab. 5 ID 4).

### 4.5 Loss

#### 4.5.1 BEV Camera-only Detection

One of the versatile benefits from BEV feature representation is to enable models to be trained with losses proposed in both 2D and 3D object detection. As reported in Tab. 4 ID 16-20, when leveraging different head design, we conclude that the corresponding losses could be transferred with minimum modification, e.g. a tuning in the loss weight.

Apart from the training loss for 3D target, auxiliary loss plays an important role in Camera-only BEV detection. One type of auxiliary loss is to add 2D detection loss on top of 2D feature extractors. Such supervision enhances the localization on 2D image feature, which in turn contributes to 3D representations provided by view transformation in BEV perception. One example of utilizing such auxiliary loss can be observed in Tab. 4 ID 4. Another type of auxiliary loss is depth supervision [49]. When utilizing ground truth depth generated from LiDAR systems, the implicit depth estimation capability of BEV perception can be improved to obtain accurate 3D object localization. Both of these auxiliary tasks can be applied during training to improve performance. As a side note, 2D detection or depth pretrained backbone are commonly adopted as initialization weights [4, 86].

#### 4.5.2 LiDAR segmentation

Instead of a conventional cross-entropy loss, Geo loss [138] and Lovász loss [139] are utilized to train all models. To have a better boundary of different classes, Geo loss has a strong response to the voxels with rich details. Lovász loss serves as a differentiable intersection-over-union (IoU) loss to mitigate the class imbalance problem. It improves the model performance by 0.6 mIoU as shown in Tab. 5 ID 2.

### 4.6 Ensemble

#### 4.6.1 BEV Camera-only Detection

The ensemble technique usually varies among datasets to be tested on; the general practice used in 2D/3D object detection could be applied to BEV perception with some modification. Take BEVFormer++ for example, in the ensemble

TABLE 6: **BEV Camera detection track.** Performance of expert models. Abbreviation and experiment IDs are inherited from Tab. 4. The overall LET-mAPL metrics and that on each category or each time-of-day subset of the models are listed in the table. Expert 1 is class rebalanced and Expert 2 is time rebalanced. D/D is short for dawn/dusk.

ID	Head	LET-mAPL						
		Overall	Car	Cyc	Ped	Day	Night	D/D
19	DeD	48.4	60.4	37.0	47.8	49.2	37.0	49.5
19.1	expert 1	48.9	61.3	37.1	48.3	-	-	-
19.2	expert 2	48.7	-	-	-	49.5	36.2	49.9
20	FrA	47.2	62.7	36.7	42.1	48.4	33.4	46.0
20.1	expert 1	47.2	62.8	36.6	42.3	-	-	-
20.2	expert 2	47.0	-	-	-	48.5	33.3	46.3
22	CeP	41.9	56.8	29.7	39.3	42.8	31.9	42.2
22.1	expert 1	42.4	57.2	30.8	39.2	-	-	-
22.2	expert 2	42.3	-	-	-	43.2	31.8	42.1

TABLE 7: **BEV Camera detection track.** Ensemble strategies on val set in BEVFormer++. FrA (FreeAnchor head [137]). DeD (Deformable DETR head [135]). CeP (Centerpoint head [67]). “20 models” denotes expert models under 20 different settings.

Head	LET-mAPL	LET-mAP	LET-mAPH
FrA	47.6	61.4	57.0
+DeD	49.1	65.2	60.2
+CeP	50.6	66.5	61.2
20 models	53.2	69.3	64.9
+Two-Stage	53.9	69.2	64.5

phase, we introduce the improved version of the weighted box fusion (WBF) [140]. Inspired by Adj-NMS [141], matrix NMS [142] is adopted following the original WBF to filter out redundant boxes. In order to generate multi-scale and flip results, a two-stage ensemble strategy is adopted. In the first stage, we utilize improved WBF to integrate predictions from the multi-scale pipeline to generate flip and non-flip results for each model. Related experiments of expert model performance are listed in Tab. 6. In the second stage, results from all expert models are gathered. The improved WBF is used to get the final results. This two-stage ensemble strategy improves the model performance by 0.7 LET-mAPL as shown in Tab. 7.

Considering the diversity of performance in each model, we argue that the parameter adjustment is much more complex. Hence the evolution algorithm is adopted to search WBF parameters and model weights. We utilize evolution in NNI [143] to automatically search parameters, where the population size is 100. The search process is based on the performance of the 3000 validation images; different classes are searched separately.

#### 4.6.2 LiDAR Segmentation

As a per-point classification task, the task of segmentation ensembles per-point probabilities from different models in an average manner. Specifically, probabilities predicted by different models are simply summed, and then per-point classification results are determined with an *argmax* operation. To improve the diversity of our models, models are

trained using a different data resampling strategy called the export model. According to context information about scenes and weather conditions, multiple context-specific models are finetuned on the model trained on all data. As shown in Tab. 5 ID 8 & 9, the usage of model ensemble and expert model brings an improvement of 0.7 and 0.3 mIoU respectively.

The probabilities of models are aggregated in a hierarchical manner after model-specific TTA. Considering the diversity of models, the model ensemble is processed in two stages. In the first stage, probabilities of homogeneous models, such as models with different hyper-parameters, are averaged with different weights. Then, probabilities of heterogeneous models, namely models with different architectures, are averaged with different weights in the second stage. Annealing algorithm with the maximum trial number 160 in NNI [143] is utilized to search weights on validation set in both stages.

## 4.7 Post-Processing

### 4.7.1 BEV Camera-only Detection

While BEV detection removes the burden of multi-camera object level fusion, we observe distinguished fact that can benefit from further post-processing. By nature of BEV transformation, duplicate features are likely to be sampled on different BEV locations along a light ray to camera center. This results in duplicate false detection on one foreground objects, where every false detection have different depth but can all be projected back to the same foreground objects in the image space. To alleviate this issue, it is beneficial to leverage 2D detection results for duplicate removal on 3D detection results, where 2D bounding boxes and 3D bounding boxes are bipartite matched. In our experiments, the 3D detection performance can be improved when using ground truth 2D bounding boxes as the filter. However, when using predicted 2D bounding boxes from the 2D detection head trained with auxiliary supervision as mentioned in Sec. 4.5.1, we observe that improvements can be barely obtained. This could be caused by the insufficient training of the 2D detection. Therefore, further investigation of the joint 2D/3D redundant detection removal is in demand.

NMS could be applied depending on whether the detection head design behaves NMS-free property. Usually, for one-to-many assignment, NMS is necessary. Notably, replacing commonly used IoU metric in NMS with the newly proposed LET-IoU [61] to remove redundant results can improve detection results. The improvements can be witnessed in Tab. 4 ID 12 & 17 & 21. This design is more suitable for BEV camera-only 3D detectors. Since the 3D IoU of two mutually redundant results is numerically small, this often leads to failure in removing false positive results. With LET-IoU, redundant results tend to obsess higher IoU, thus being removed to a great extent.

### 4.7.2 LiDAR Segmentation

By analyzing the confusion matrix, we observe that most misclassification occurs within similar classes. Thus, semantic classes can be divided into groups, in which classes are intensively confused compared to classes outside the group. Post-processing techniques are conducted on foreground

semantic groups separately, and bring an improvement of 0.9 mIoU in Tab. 5 ID 10.

Existing segmentation methods perform per-point classification, without considering the consistency of a single object. For instance, some points labeled as foreground objects would be predicted as background. Object-level refinement is conducted to further improve object-level integrity based on the aforementioned hierarchical classification. By masking points in the same semantic group based on prediction and performing Euclidean clustering, points could be grouped into instances. Then the prediction of each instance is determined by majority voting. Besides, for each object, the justification of object-level classification is performed by a lightweight classification network to determine the ultimate predicted class of the object.

As object-level prediction is obtained, the time consistency of the prediction is further refined by tracking. Tracking is performed to find the corresponding object from all previous frames. The predicted class of an object in the current frame is refined by considering all previous predictions.

## 5 CONCLUSION

In this survey, we conduct a thorough review on BEV perception in recent years and provide a practical recipe according to our analysis in BEV design pipeline. Grand challenges and future endeavors could be: (a) how to devise a more accurate depth estimator; (b) how to better align feature representations from multiple sensors in a novel fusion mechanism; (c) how to design a parameter-free network such that the algorithm performance is free to pose variation or sensor location, achieving better generalization ability across various scenarios; and (d) how to incorporate the successful knowledge from foundation models to facilitate BEV perception. More detailed discussion could be found in the Appendix. We hope this survey can benefit the community and be an insightful cookbook for later research in 3D perception.

## ACKNOWLEDGMENTS

The authors would like to thank Xiaogang Wang, Tai Wang, Yu Liu for fruitful idea discussions and Conghui He, Li Liu, Jin Yu, Zhenming Xiao, Qian Liu for coordinating the data processing pipeline. We thank SenseTime for the GPU support during Waymo challenge. Our special thanks go to the Waymo challenge team members for their contribution to the experiments, including Yangyi Huang, Jiawei Li, Tianyu Li, Wenkang Qin and Yan Bai. We would also like to thank Jiangwei Xie for maintaining the repository associated with bag of tricks mentioned in this report.

## REFERENCES

- [1] S. Ren, K. He, R. Girshick, and J. Sun, "Faster R-CNN: Towards real-time object detection with region proposal networks," *IEEE Transactions on Pattern Analysis and Machine Intelligence*, vol. 39, no. 6, pp. 1137–1149, 2017.
- [2] K. He, G. Gkioxari, P. Dollár, and R. Girshick, "Mask R-CNN," in *IEEE Conference on Computer Vision and Pattern Recognition*, 2017.

- [3] E. Xie, Z. Yu, D. Zhou, J. Philion, A. Anandkumar, S. Fidler, P. Luo, and J. M. Alvarez, "M<sup>2</sup>BEV: Multi-camera joint 3d detection and segmentation with unified birds-eye view representation," *arXiv preprint arXiv:2204.05088*, 2022.
- [4] Z. Li, W. Wang, H. Li, E. Xie, C. Sima, T. Lu, Q. Yu, and J. Dai, "BEVFormer: Learning bird's-eye-view representation from multi-camera images via spatiotemporal transformers," *arXiv preprint arXiv:2203.17270*, 2022.
- [5] Z. Liu, H. Tang, A. Amini, X. Yang, H. Mao, D. Rus, and S. Han, "BEVFusion: Multi-task multi-sensor fusion with unified bird's-eye view representation," *arXiv preprint arXiv:2205.13542*, 2022.
- [6] (2021) Tesla AI Day. [Online]. Available: <https://www.youtube.com/watch?v=j0z4FweCy4M>
- [7] H. Caesar, V. Bankiti, A. H. Lang, S. Vora, V. E. Liong, Q. Xu, A. Krishnan, Y. Pan, G. Baldan, and O. Beijbom, "nuscenes: A multimodal dataset for autonomous driving," in *IEEE Conference on Computer Vision and Pattern Recognition*, 2020.
- [8] P. Sun, H. Kretzschmar, X. Dotiwalla, A. Chouard, V. Patnaik, P. Tsui, J. Guo, Y. Zhou, Y. Chai, B. Caine, V. Vasudevan, W. Han, J. Ngiam, H. Zhao, A. Timofeev, S. Ettinger, M. Krivokon, A. Gao, A. Joshi, Y. Zhang, J. Shlens, C. Zhifeng, and D. Anguelov, "Scalability in perception for autonomous driving: Waymo open dataset," in *IEEE Conference on Computer Vision and Pattern Recognition*, 2020.
- [9] H. Chen, P. Wang, F. Wang, W. Tian, L. Xiong, and H. Li, "EPro-PnP: Generalized end-to-end probabilistic perspective-n-points for monocular object pose estimation," in *IEEE Conference on Computer Vision and Pattern Recognition*, 2022.
- [10] T. Wang, J. Pang, and D. Lin, "Monocular 3d object detection with depth from motion," *arXiv preprint arXiv:2207.12988*, 2022.
- [11] A. Geiger, P. Lenz, and R. Urtasun, "Are we ready for autonomous driving? the kitti vision benchmark suite," in *IEEE Conference on Computer Vision and Pattern Recognition*, 2012.
- [12] B. Wilson, W. Qi, T. Agarwal, J. Lambert, J. Singh, S. Khandelwal, B. Pan, R. Kumar, A. Hartnett, J. K. Pontes, D. Ramanan, P. Carr, and J. Hays, "Argoverse 2: Next generation datasets for self-driving perception and forecasting," in *Neural Information Processing Systems Track on Datasets and Benchmarks*, 2021.
- [13] (2020) Drago Anguelov – Machine Learning for Autonomous Driving at Scale. [Online]. Available: <https://youtu.be/BV4EXwlb3yo>
- [14] A. Vaswani, N. Shazeer, N. Parmar, J. Uszkoreit, L. Jones, A. N. Gomez, L. Kaiser, and I. Polosukhin, "Attention is all you need," in *Advances in Neural Information Processing Systems*, 2017.
- [15] A. Dosovitskiy, L. Beyer, A. Kolesnikov, D. Weissenborn, X. Zhai, T. Unterthiner, M. Dehghani, M. Minderer, G. Heigold, S. Gelly, J. Uszkoreit, and N. Houlsby, "An image is worth 16x16 words: Transformers for image recognition at scale," *arXiv preprint arXiv:2010.11929*, 2020.
- [16] K. Han, Y. Wang, H. Chen, X. Chen, J. Guo, Z. Liu, Y. Tang, A. Xiao, C. Xu, Y. Xu *et al.*, "A survey on vision transformer," *IEEE transactions on pattern analysis and machine intelligence*, 2022.
- [17] K. He, X. Chen, S. Xie, Y. Li, P. Dollár, and R. Girshick, "Masked autoencoders are scalable vision learners," in *IEEE Conference on Computer Vision and Pattern Recognition*, 2022.
- [18] A. Radford, J. W. Kim, C. Hallacy, A. Ramesh, G. Goh, S. Agarwal, G. Sastry, A. Askell, P. Mishkin, J. Clark, G. Krueger, and I. Sutskever, "Learning transferable visual models from natural language supervision," in *International Conference on Machine Learning*, 2021.
- [19] E. Arnold, O. Y. Al-Jarrah, M. Dianati, S. Fallah, D. Oxtoby, and A. Mouzakitis, "A survey on 3d object detection methods for autonomous driving applications," *IEEE Transactions on Intelligent Transportation Systems*, vol. 20, no. 10, pp. 3782–3795, 2019.
- [20] W. Liang, P. Xu, L. Guo, H. Bai, Y. Zhou, and F. Chen, "A survey of 3d object detection," *Multimedia Tools and Applications*, vol. 80, no. 19, pp. 29 617–29 641, 2021.
- [21] R. Qian, X. Lai, and X. Li, "3d object detection for autonomous driving: a survey," *Pattern Recognition*, p. 108796, 2022.
- [22] Y. Ma, T. Wang, X. Bai, H. Yang, Y. Hou, Y. Wang, Y. Qiao, R. Yang, D. Manocha, and X. Zhu, "Vision-centric bev perception: A survey," *arXiv preprint arXiv:2208.02797*, 2022.
- [23] J. Mao, S. Shi, X. Wang, and H. Li, "3d object detection for autonomous driving: A review and new outlooks," *arXiv preprint arXiv:2206.09474*, 2022.
- [24] M.-F. Chang, J. W. Lambert, P. Sangkloy, J. Singh, S. Bak, A. Hartnett, D. Wang, P. Carr, S. Lucey, D. Ramanan, and J. Hays, "Argoverse: 3d tracking and forecasting with rich maps," in *IEEE Conference on Computer Vision and Pattern Recognition*, 2019.
- [25] X. Huang, P. Wang, X. Cheng, D. Zhou, Q. Geng, and R. Yang, "The apolloscape open dataset for autonomous driving and its application," *IEEE transactions on pattern analysis and machine intelligence*, vol. 42, no. 10, pp. 2702–2719, 2019.
- [26] L. Chen, C. Sima, Y. Li, Z. Zheng, J. Xu, X. Geng, H. Li, C. He, J. Shi, Y. Qiao, and J. Yan, "PersFormer: 3d lane detection via perspective transformer and the openlane benchmark," *arXiv preprint arXiv:2203.11089*, 2022.
- [27] F. Yan, M. Nie, X. Cai, J. Han, H. Xu, Z. Yang, C. Ye, Y. Fu, M. B. Mi, and L. Zhang, "Once-3dlanes: Building monocular 3d lane detection," in *Proceedings of the IEEE/CVF Conference on Computer Vision and Pattern Recognition*, 2022, pp. 17 143–17 152.
- [28] J. Houston, G. Zuidhof, L. Bergamini, Y. Ye, L. Chen, A. Jain, S. Omari, V. Iglovikov, and P. Ondruska, "One thousand and one hours: Self-driving motion prediction dataset," in *Conference on Robot Learning*, 2020.
- [29] Q.-H. Pham, P. Sevestre, R. S. Pahwa, H. Zhan, C. H. Pang, Y. Chen, A. Mustafa, V. Chandrasekhar, and J. Lin, "A\* 3d dataset: Towards autonomous driving in challenging environments," in *IEEE International Conference on Robotics and Automation*, 2020.
- [30] A. Patil, S. Malla, H. Gang, and Y.-T. Chen, "The h3d dataset for full-surround 3d multi-object detection and tracking in crowded urban scenes," in *IEEE International Conference on Robotics and Automation*, 2019.
- [31] J. Behley, M. Garbade, A. Milioto, J. Quenzel, S. Behnke, C. Stachniss, and J. Gall, "SemanticKITTI: A Dataset for Semantic Scene Understanding of LiDAR Sequences," in *IEEE International Conference on Computer Vision*, 2019.
- [32] J. Geyer, Y. Kassahun, M. Mahmudi, X. Ricou, R. Durgesh, A. S. Chung, L. Hauswald, V. H. Pham, M. Mühlegg, S. Dorn *et al.*, "A2d2: Audi autonomous driving dataset," *arXiv preprint arXiv:2004.06320*, 2020.
- [33] N. Ghlert, N. Jourdan, M. Cordts, U. Franke, and J. Denzler, "Cityscapes 3d: Dataset and benchmark for 9 dof vehicle detection," *arXiv preprint arXiv:2006.07864*, 2020.
- [34] P. Xiao, Z. Shao, S. Hao, Z. Zhang, X. Chai, J. Jiao, Z. Li, J. Wu, K. Sun, K. Jiang *et al.*, "Pandaset: Advanced sensor suite dataset for autonomous driving," in *IEEE International Intelligent Transportation Systems Conference*, 2021.
- [35] Y. Liao, J. Xie, and A. Geiger, "KITTI-360: A novel dataset and benchmarks for urban scene understanding in 2d and

- 3d," *arXiv preprint arXiv:2109.13410*, 2021.
- [36] Z. Wang, S. Ding, Y. Li, J. Fenn, S. Roychowdhury, A. Wallin, L. Martin, S. Rylvola, G. Sapiro, and Q. Qiu, "Cirrus: A long-range bi-pattern lidar dataset," in *IEEE International Conference on Robotics and Automation*, 2021.
- [37] J. Mao, M. Niu, C. Jiang, X. Liang, Y. Li, C. Ye, W. Zhang, Z. Li, J. Yu, C. Xu *et al.*, "One million scenes for autonomous driving: Once dataset," *arXiv preprint arXiv:2106.11037*, 2021.
- [38] X. Weng, Y. Man, J. Park, Y. Yuan, D. Cheng, M. O'Toole, and K. Kitani, "All-In-One Drive: A Large-Scale Comprehensive Perception Dataset with High-Density Long-Range Point Clouds," *arXiv*, 2021.
- [39] T. Wang, W. Ji, S. Chen, G. Chongjian, E. Xie, and P. Luo, "DeepAccident: A large-scale accident dataset for multi-vehicle autonomous driving," 2022.
- [40] A. Dosovitskiy, G. Ros, F. Codevilla, A. Lopez, and V. Koltun, "Carla: An open urban driving simulator," in *Conference on Robot Learning*, 2017.
- [41] S. Song, S. P. Lichtenberg, and J. Xiao, "SUN RGB-D: A rgb-d scene understanding benchmark suite," in *IEEE Conference on Computer Vision and Pattern Recognition*, 2015.
- [42] A. Dai, A. X. Chang, M. Savva, M. Halber, T. Funkhouser, and M. Nießner, "ScanNet: Richly-annotated 3d reconstructions of indoor scenes," in *IEEE Conference on Computer Vision and Pattern Recognition*, 2017.
- [43] T. Roddick, A. Kendall, and R. Cipolla, "Orthographic feature transform for monocular 3d object detection," in *British Machine Vision Conference*, 2019.
- [44] Y. Zhou and O. Tuzel, "Voxelnet: End-to-end learning for point cloud based 3d object detection," in *IEEE Conference on Computer Vision and Pattern Recognition*, 2018.
- [45] A. H. Lang, S. Vora, H. Caesar, L. Zhou, J. Yang, and O. Beijbom, "Pointpillars: Fast encoders for object detection from point clouds," in *IEEE Conference on Computer Vision and Pattern Recognition*, 2019.
- [46] C. Reading, A. Harakeh, J. Chae, and S. L. Waslander, "Categorical depth distribution network for monocular 3d object detection," in *IEEE Conference on Computer Vision and Pattern Recognition*, 2021.
- [47] J. Huang, G. Huang, Z. Zhu, and D. Du, "BEVDet: High-performance multi-camera 3d object detection in bird-eye-view," *arXiv preprint arXiv:2112.11790*, 2021.
- [48] Y. Liu, T. Wang, X. Zhang, and J. Sun, "Petr: Position embedding transformation for multi-view 3d object detection," *arXiv preprint arXiv:2203.05625*, 2022.
- [49] Y. Li, Z. Ge, G. Yu, J. Yang, Z. Wang, Y. Shi, J. Sun, and Z. Li, "BEVDepth: Acquisition of reliable depth for multi-view 3d object detection," *arXiv preprint arXiv:2206.10092*, 2022.
- [50] D. Rukhovich, A. Vorontsova, and A. Konushin, "Imvoxelnet: Image to voxels projection for monocular and multi-view general-purpose 3d object detection," in *IEEE/CVF Winter Conference on Applications of Computer Vision*, 2022.
- [51] Y. Jiang, L. Zhang, Z. Miao, X. Zhu, J. Gao, W. Hu, and Y.-G. Jiang, "Polarformer: Multi-camera 3d object detection with polar transformers," *arXiv preprint arXiv:2206.15398*, 2022.
- [52] L. Reiher, B. Lampe, and L. Eckstein, "A sim2real deep learning approach for the transformation of images from multiple vehicle-mounted cameras to a semantically segmented image in bird's eye view," in *IEEE 23rd International Conference on Intelligent Transportation Systems*, 2020.
- [53] A. Hu, Z. Murez, N. Mohan, S. Dudas, J. Hawke, V. Badrinarayanan, R. Cipolla, and A. Kendall, "FIERY: Future instance prediction in bird's-eye view from surround monocular cameras," in *IEEE International Conference on Computer Vision*, 2021.
- [54] B. Zhou and P. Krähenbühl, "Cross-view transformers for real-time map-view semantic segmentation," in *IEEE Conference on Computer Vision and Pattern Recognition*, 2022.
- [55] Q. Li, Y. Wang, Y. Wang, and H. Zhao, "Hdmapnet: An online hd map construction and evaluation framework," in *IEEE International Conference on Robotics and Automation*, 2022.
- [56] A. Saha, O. Mendez, C. Russell, and R. Bowden, "Translating images into maps," in *IEEE International Conference on Robotics and Automation*, 2022.
- [57] J. Philion and S. Fidler, "Lift, splat, shoot: Encoding images from arbitrary camera rigs by implicitly unprojecting to 3d," in *European Conference on Computer Vision*, 2020.
- [58] S. Hu, L. Chen, P. Wu, H. Li, J. Yan, and D. Tao, "ST-P3: End-to-end vision-based autonomous driving via spatial-temporal feature learning," *arXiv preprint arXiv:2207.07601*, 2022.
- [59] N. Garnett, R. Cohen, T. Pe'er, R. Lahav, and D. Levi, "3d-lanenet: end-to-end 3d multiple lane detection," in *IEEE International Conference on Computer Vision*, 2019.
- [60] Y. B. Can, A. Liniger, D. P. Paudel, and L. Van Gool, "Structured bird's-eye-view traffic scene understanding from onboard images," in *IEEE International Conference on Computer Vision*, 2021.
- [61] W.-C. Hung, H. Kretschmar, V. Casser, J.-J. Hwang, and D. Anguelov, "Let-3d-ap: Longitudinal error tolerant 3d average precision for camera-only 3d detection," *arXiv preprint arXiv:2206.07705*, 2022.
- [62] T. Wang, Z. Xinge, J. Pang, and D. Lin, "Probabilistic and geometric depth: Detecting objects in perspective," in *Conference on Robot Learning*, 2022.
- [63] Y. Zhang, Z. Zhu, W. Zheng, J. Huang, G. Huang, J. Zhou, and J. Lu, "BEVerse: Unified perception and prediction in birds-eye-view for vision-centric autonomous driving," *arXiv preprint arXiv:2205.09743*, 2022.
- [64] J. Huang and G. Huang, "BEVDet4D: Exploit temporal cues in multi-camera 3d object detection," *arXiv preprint arXiv:2203.17054*, 2022.
- [65] C. Yilun, S. Liu, X. Shen, and J. Jia, "Dsgn: Deep stereo geometry network for 3d object detection," *IEEE Conference on Computer Vision and Pattern Recognition*, 2020.
- [66] S. Shi, C. Guo, L. Jiang, Z. Wang, J. Shi, X. Wang, and H. Li, "PV-RCNN: Point-voxel feature set abstraction for 3d object detection," in *IEEE Conference on Computer Vision and Pattern Recognition*, 2020, pp. 10 529–10 538.
- [67] T. Yin, X. Zhou, and P. Krahenbuhl, "Center-based 3d object detection and tracking," in *IEEE Conference on Computer Vision and Pattern Recognition*, 2021.
- [68] L. Fan, Z. Pang, T. Zhang, Y.-X. Wang, H. Zhao, F. Wang, N. Wang, and Z. Zhang, "Embracing single stride 3d object detector with sparse transformer," in *IEEE Conference on Computer Vision and Pattern Recognition*, 2022.
- [69] Y. Hu, Z. Ding, R. Ge, W. Shao, L. Huang, K. Li, and Q. Liu, "AFDetV2: Rethinking the necessity of the second stage for object detection from point clouds," *AAAI Conference on Artificial Intelligence*, 2022.
- [70] S. Shi, L. Jiang, J. Deng, Z. Wang, C. Guo, J. Shi, X. Wang, and H. Li, "PV-RCNN++: Point-voxel feature set abstraction with local vector representation for 3d object detection," *arXiv preprint arXiv:2102.00463*, 2021.
- [71] J. Mao, M. Niu, H. Bai, X. Liang, H. Xu, and C. Xu, "Pyramid R-CNN: Towards better performance and adaptability for 3d object detection," in *IEEE International Conference on Computer Vision*, 2021.
- [72] X. Chen, S. Shi, B. Zhu, K. C. Cheung, H. Xu, and H. Li, "MPPNet: Multi-frame feature intertwining with proxy points for 3d temporal object detection," *arXiv preprint arXiv:2205.05979*, 2022.

- [73] S. Vora, A. H. Lang, B. Helou, and O. Beijbom, "PointPainting: Sequential fusion for 3d object detection," in *IEEE Conference on Computer Vision and Pattern Recognition*, 2020.
- [74] T. Yin, X. Zhou, and P. Krhenbhl, "Multimodal virtual point 3d detection," *Advances in Neural Information Processing Systems*, 2021.
- [75] Z. Chen, Z. Li, S. Zhang, L. Fang, Q. Jiang, F. Zhao, B. Zhou, and H. Zhao, "AutoAlign: Pixel-instance feature aggregation for multi-modal 3d object detection," *arXiv preprint arXiv:2201.06493*, 2022.
- [76] X. Bai, Z. Hu, X. Zhu, Q. Huang, Y. Chen, H. Fu, and C.-L. Tai, "TransFusion: Robust lidar-camera fusion for 3d object detection with transformers," in *IEEE Conference on Computer Vision and Pattern Recognition*, 2022.
- [77] Y. Li, A. W. Yu, T. Meng, B. Caine, J. Ngiam, D. Peng, J. Shen, B. Wu, Y. Lu, D. Zhou, Q. V. Le, A. Yuille, and M. Tan, "Deepfusion: Lidar-camera deep fusion for multi-modal 3d object detection," in *IEEE Conference on Computer Vision and Pattern Recognition*, 2022.
- [78] Z. Chen, Z. Li, S. Zhang, L. Fang, Q. Jiang, and F. Zhao, "AutoAlignV2: Deformable feature aggregation for dynamic multi-modal 3d object detection," *arXiv preprint arXiv:2207.10316*, 2022.
- [79] K. He, R. Girshick, and P. Dollr, "Rethinking imagenet pre-training," in *IEEE International Conference on Computer Vision*, 2019.
- [80] T.-Y. Lin, P. Dollr, R. B. Girshick, K. He, B. Hariharan, and S. J. Belongie, "Feature pyramid networks for object detection," *IEEE Conference on Computer Vision and Pattern Recognition*, 2017.
- [81] D. Park, R. Ambrus, V. Guizilini, J. Li, and A. Gaidon, "Is pseudo-lidar needed for monocular 3d object detection?" in *IEEE International Conference on Computer Vision*, 2021.
- [82] T. Wang, X. Zhu, J. Pang, and D. Lin, "FCOS3D: Fully convolutional one-stage monocular 3d object detection," in *IEEE International Conference on Computer Vision*, 2021, pp. 913–922.
- [83] Z. Liu, Z. Wu, and R. Tth, "SMOKE: Single-stage monocular 3d object detection via keypoint estimation," *arXiv preprint arXiv:2002.10111*, 2020.
- [84] H. Tang, Z. Liu, S. Zhao, Y. Lin, J. Lin, H. Wang, and S. Han, "Searching efficient 3d architectures with sparse point-voxel convolution," in *European Conference on Computer Vision*, 2020.
- [85] Y. Yan, Y. Mao, and B. Li, "Second: Sparsely embedded convolutional detection," *Sensors*, vol. 18, no. 10, p. 3337, 2018.
- [86] Y. Wang, V. C. Guizilini, T. Zhang, Y. Wang, H. Zhao, and J. Solomon, "Det3d: 3d object detection from multi-view images via 3d-to-2d queries," in *Conference on Robot Learning*, 2022.
- [87] F. Li, H. Zhang, S. Liu, J. Guo, L. M. Ni, and L. Zhang, "Dn-detr: Accelerate detr training by introducing query denoising," in *IEEE Conference on Computer Vision and Pattern Recognition*, 2022.
- [88] D. Meng, X. Chen, Z. Fan, G. Zeng, H. Li, Y. Yuan, L. Sun, and J. Wang, "Conditional detr for fast training convergence," in *IEEE International Conference on Computer Vision*, 2021.
- [89] Y. Wang, W.-L. Chao, D. Garg, B. Hariharan, M. Campbell, and K. Q. Weinberger, "Pseudo-lidar from visual depth estimation: Bridging the gap in 3d object detection for autonomous driving," in *IEEE Conference on Computer Vision and Pattern Recognition*, 2019.
- [90] Y. You, Y. Wang, W.-L. Chao, D. Garg, G. Pleiss, B. Hariharan, M. Campbell, and K. Q. Weinberger, "Pseudo-lidar++: Accurate depth for 3d object detection in autonomous driving," *arXiv preprint arXiv:1906.06310*, 2019.
- [91] T. Liang, H. Xie, K. Yu, Z. Xia, Z. Lin, Y. Wang, T. Tang, B. Wang, and Z. Tang, "BEVFusion: A simple and robust lidar-camera fusion framework," *arXiv preprint arXiv:2205.13790*, 2022.
- [92] X. Guo, S. Shi, X. Wang, and H. Li, "LIGA-Stereo: Learning lidar geometry aware representations for stereo-based 3d detector," *IEEE International Conference on Computer Vision*, 2021.
- [93] H. A. Mallot, H. H. Blthoff, J. Little, and S. Bohrer, "Inverse perspective mapping simplifies optical flow computation and obstacle detection," *Biological cybernetics*, vol. 64, no. 3, pp. 177–185, 1991.
- [94] A. M. Andrew, "Multiple view geometry in computer vision," *Kybernetes*, 2001.
- [95] A. Vaswani, N. Shazeer, N. Parmar, J. Uszkoreit, L. Jones, A. N. Gomez, . Kaiser, and . Polosukhin, "Attention is all you need," in *Advances in Neural Information Processing Systems*, 2017.
- [96] S. Gong, X. Ye, X. Tan, J. Wang, E. Ding, Y. Zhou, and X. Bai, "GitNet: Geometric prior-based transformation for birds-eye-view segmentation," *arXiv preprint arXiv:2204.07733*, 2022.
- [97] T. Wang, Q. Lian, C. Zhu, X. Zhu, and W. Zhang, "MV-FCOS3D++: Multi-View camera-only 4d object detection with pretrained monocular backbones," *arXiv preprint*, 2022.
- [98] Z. Tian, C. Shen, H. Chen, and T. He, "FCOS: Fully convolutional one-stage object detection," in *IEEE International Conference on Computer Vision*, 2019.
- [99] R. Girshick, "Fast R-CNN," in *IEEE International Conference on Computer Vision*, 2015.
- [100] B. Xu and Z. Chen, "Multi-level fusion based 3d object detection from monocular images," in *IEEE Conference on Computer Vision and Pattern Recognition*, 2018.
- [101] M. H. Ng, K. Radia, J. Chen, D. Wang, I. Gog, and J. E. Gonzalez, "BEV-Seg: Bird's eye view semantic segmentation using geometry and semantic point cloud," *arXiv preprint arXiv:2006.11436*, 2020.
- [102] C. R. Qi, H. Su, K. Mo, and L. J. Guibas, "PointNet: Deep learning on point sets for 3d classification and segmentation," in *IEEE Conference on Computer Vision and Pattern Recognition*, 2017.
- [103] C. R. Qi, L. Yi, H. Su, and L. J. Guibas, "PointNet++: Deep hierarchical feature learning on point sets in a metric space," in *Advances in Neural Information Processing Systems*, 2017.
- [104] C. He, H. Zeng, J. Huang, X.-S. Hua, and L. Zhang, "Structure aware single-stage 3d object detection from point cloud," in *IEEE Conference on Computer Vision and Pattern Recognition*, 2020.
- [105] J. Mao, Y. Xue, M. Niu, H. Bai, J. Feng, X. Liang, H. Xu, and C. Xu, "Voxel transformer for 3d object detection," in *IEEE International Conference on Computer Vision*, 2021.
- [106] J. Deng, S. Shi, P. Li, W. Zhou, Y. Zhang, and H. Li, "Voxel R-CNN: Towards high performance voxel-based 3d object detection," in *AAAI Conference on Artificial Intelligence*, 2021.
- [107] Y. Wang and J. M. Solomon, "Object dgcnn: 3d object detection using dynamic graphs," in *Advances in Neural Information Processing Systems*, M. Ranzato, A. Beygelzimer, Y. Dauphin, P. Liang, and J. W. Vaughan, Eds., 2021.
- [108] X. Chen, H. Ma, J. Wan, B. Li, and T. Xia, "Multi-view 3d object detection network for autonomous driving," in *IEEE Conference on Computer Vision and Pattern Recognition*, 2017.
- [109] B. Yang, W. Luo, and R. Urtasun, "PIXOR: Real-time 3d object detection from point clouds," in *IEEE Conference on Computer Vision and Pattern Recognition*, 2018.
- [110] B. Yang, M. Liang, and R. Urtasun, "Hdnet: Exploiting hd maps for 3d object detection," in *Conference on Robot Learning*, 2018.

- [111] J. Beltrán, C. Guindel, F. M. Moreno, D. Cruzado, F. García, and A. De La Escalera, "BirdNet: A 3d object detection framework from lidar information," in *International Conference on Intelligent Transportation Systems*, 2018.
- [112] Y. Zeng, Y. Hu, S. Liu, J. Ye, Y. Han, X. Li, and N. Sun, "Rt3d: Real-time 3-d vehicle detection in lidar point cloud for autonomous driving," *IEEE Robotics and Automation Letters*, vol. 3, no. 4, pp. 3434–3440, 2018.
- [113] W. Ali, S. Abdelkarim, M. Zidan, M. Zahran, and A. El Sallab, "Yolo3d: End-to-end real-time 3d oriented object bounding box detection from lidar point cloud," in *European Conference on Computer Vision Workshops*, 2018.
- [114] M. Simony, S. Milzy, K. Amendey, and H.-M. Gross, "Complex-YOLO: An euler-region-proposal for real-time 3d object detection on point clouds," in *European Conference on Computer Vision Workshops*, 2018.
- [115] K. He, X. Zhang, S. Ren, and J. Sun, "Deep residual learning for image recognition," in *IEEE Conference on Computer Vision and Pattern Recognition*, 2016.
- [116] B. Graham, "Spatially-sparse convolutional neural networks," *arXiv preprint arXiv:1409.6070*, 2014.
- [117] C. Choy, J. Gwak, and S. Savarese, "4d spatio-temporal convnets: Minkowski convolutional neural networks," in *IEEE Conference on Computer Vision and Pattern Recognition*, 2019.
- [118] C. R. Qi, O. Litany, K. He, and L. J. Guibas, "Deep hough voting for 3d object detection in point clouds," in *IEEE International Conference on Computer Vision*, 2019.
- [119] X. Pan, Z. Xia, S. Song, L. E. Li, and G. Huang, "3d object detection with pointformer," in *IEEE Conference on Computer Vision and Pattern Recognition*, 2021.
- [120] H. Mallot, H. Bülthoff, J. Little, and S. Bohrer, "Inverse perspective mapping simplifies optical flow computation and obstacle detection," *Biological Cybernetics*, vol. 64, no. 3, pp. 177–185, 1991.
- [121] Y. Li, Y. Chen, X. Qi, Z. Li, J. Sun, and J. Jia, "Unifying voxel-based representation with transformer for 3d object detection," *arXiv preprint arXiv:2206.00630*, 2022.
- [122] C. Wang, C. Ma, M. Zhu, and X. Yang, "PointAugmenting: Cross-modal augmentation for 3d object detection," in *IEEE Conference on Computer Vision and Pattern Recognition*, 2021.
- [123] A. Laddha, S. Gautam, S. Palombo, S. Pandey, and C. Vallespi-Gonzalez, "MVFuseNet: Improving end-to-end object detection and motion forecasting through multi-view fusion of lidar data," in *IEEE/CVF Conference on Computer Vision and Pattern Recognition Workshops*, 2021.
- [124] Z. Qin, J. Chen, C. Chen, X. Chen, and X. Li, "UniFormer: Unified multi-view fusion transformer for spatial-temporal representation in bird's-eye-view," *arXiv preprint arXiv:2207.08536*, 2022.
- [125] (2022) Horizon Algorithms . [Online]. Available: <https://en.horizon.ai/products/applications-algorithms/>
- [126] (2022) HAOMO AI DAY . [Online]. Available: <https://www.bilibili.com/video/BV1Wr4y1H7W7>
- [127] (2022) PhiGent: Technical Roadmap . [Online]. Available: <https://43.132.128.84/coreTechnology>
- [128] (2020) CES 2020 by Mobileye . [Online]. Available: <https://youtu.be/HPWGFzqd7pI>
- [129] I. Radosavovic, R. P. Kosaraju, R. Girshick, K. He, and P. Dollár, "Designing network design spaces," in *IEEE Conference on Computer Vision and Pattern Recognition*, 2020.
- [130] M. Tan, R. Pang, and Q. V. Le, "EfficientDet: Scalable and efficient object detection," in *IEEE Conference on Computer Vision and Pattern Recognition*, 2020.
- [131] T. Zhou, M. Brown, N. Snavely, and D. G. Lowe, "Unsupervised learning of depth and ego-motion from video," in *IEEE Conference on Computer Vision and Pattern Recognition*, 2017.
- [132] A. Gordon, H. Li, R. Jonschkowski, and A. Angelova, "Depth from videos in the wild: Unsupervised monocular depth learning from unknown cameras," in *IEEE International Conference on Computer Vision*, 2019.
- [133] Z. Liu, Y. Lin, Y. Cao, H. Hu, Y. Wei, Z. Zhang, S. Lin, and B. Guo, "Swin transformer: Hierarchical vision transformer using shifted windows," in *IEEE International Conference on Computer Vision*, 2021.
- [134] H. Law and J. Deng, "Cornersnet: Detecting objects as paired keypoints," in *European Conference on Computer Vision*, 2018.
- [135] X. Zhu, W. Su, L. Lu, B. Li, X. Wang, and J. Dai, "Deformable detr: Deformable transformers for end-to-end object detection," in *International Conference on Learning Representations*, 2020.
- [136] N. Carion, F. Massa, G. Synnaeve, N. Usunier, A. Kirillov, and S. Zagoruyko, "End-to-end object detection with transformers," in *European Conference on Computer Vision*, 2020.
- [137] X. Zhang, F. Wan, C. Liu, R. Ji, and Q. Ye, "Freeanchor: Learning to match anchors for visual object detection," in *Advances in Neural Information Processing Systems*, 2019.
- [138] J. Li, Y. Liu, X. Yuan, C. Zhao, R. Siegwart, I. Reid, and C. Cadena, "Depth based semantic scene completion with position importance aware loss," *IEEE Robotics and Automation Letters*, vol. 5, no. 1, pp. 219–226, 2019.
- [139] M. Berman, A. R. Triki, and M. B. Blaschko, "The lovász-softmax loss: A tractable surrogate for the optimization of the intersection-over-union measure in neural networks," in *IEEE Conference on Computer Vision and Pattern Recognition*, 2018.
- [140] R. Solovyev, W. Wang, and T. Gabruseva, "Weighted boxes fusion: Ensembling boxes from different object detection models," *Image and Vision Computing*, vol. 107, pp. 104–117, 2021.
- [141] Y. Liu, G. Song, Y. Zang, Y. Gao, E. Xie, J. Yan, C. C. Loy, and X. Wang, "1st place solutions for openimage2019-object detection and instance segmentation," *arXiv preprint arXiv:2003.07557*, 2020.
- [142] X. Wang, R. Zhang, T. Kong, L. Li, and C. Shen, "SOLOv2: Dynamic and fast instance segmentation," *Advances in Neural Information Processing Systems*, 2020.
- [143] "Neural network intelligence." [Online]. Available: <https://github.com/microsoft/nni>
- [144] X. Chen, K. Kundu, Z. Zhang, H. Ma, S. Fidler, and R. Urtasun, "Monocular 3d object detection for autonomous driving," in *IEEE Conference on Computer Vision and Pattern Recognition*, 2016.
- [145] A. Mousavian, D. Anguelov, J. Flynn, and J. Kosecka, "3d bounding box estimation using deep learning and geometry," in *IEEE Conference on Computer Vision and Pattern Recognition*, 2017.
- [146] A. Kundu, Y. Li, and J. M. Rehg, "3D-RCNN: Instance-level 3d object reconstruction via render-and-compare," in *IEEE Conference on Computer Vision and Pattern Recognition*, 2018.
- [147] X. Zhou, D. Wang, and P. Krähenbühl, "Objects as points," *arXiv preprint arXiv:1904.07850*, 2019.
- [148] G. Brazil and X. Liu, "M3D-RPN: Monocular 3d region proposal network for object detection," in *IEEE International Conference on Computer Vision*, 2019.
- [149] J. Ku, A. D. Pon, and S. L. Waslander, "Monocular 3d object detection leveraging accurate proposals and shape reconstruction," in *IEEE Conference on Computer Vision and Pattern Recognition*, 2019.
- [150] F. Manhardt, W. Kehl, and A. Gaidon, "ROI-10D: Monocular lifting of 2d detection to 6d pose and metric shape," in *IEEE Conference on Computer Vision and Pattern Recognition*, 2019.

- [151] S. Shi, X. Wang, and H. Li, "PointRCNN: 3d object proposal generation and detection from point cloud," in *IEEE Conference on Computer Vision and Pattern Recognition*, 2019.
- [152] S. Shi, Z. Wang, J. Shi, X. Wang, and H. Li, "From points to parts: 3d object detection from point cloud with part-aware and part-aggregation network," *IEEE transactions on pattern analysis and machine intelligence*, vol. 43, no. 8, pp. 2647–2664, 2020.
- [153] Z. Zhang, B. Sun, H. Yang, and Q. Huang, "H3DNet: 3d object detection using hybrid geometric primitives," in *European Conference on Computer Vision*, 2020.
- [154] B. Cheng, L. Sheng, S. Shi, M. Yang, and D. Xu, "Back-tracing representative points for voting-based 3d object detection in point clouds," in *IEEE Conference on Computer Vision and Pattern Recognition*, 2021.
- [155] Z. Liu, Z. Zhang, Y. Cao, H. Hu, and X. Tong, "Group-free 3d object detection via transformers," in *IEEE International Conference on Computer Vision*, 2021.
- [156] H. Wang, S. Shi, Z. Yang, R. Fang, Q. Qian, H. Li, B. Schiele, and L. Wang, "RBGNet: Ray-based grouping for 3d object detection," in *IEEE Conference on Computer Vision and Pattern Recognition*, 2022.
- [157] Z. Yang, Y. Sun, S. Liu, and J. Jia, "3DSSD: Point-based 3d single stage object detector," in *IEEE Conference on Computer Vision and Pattern Recognition*, 2020.
- [158] Y. Xu, T. Fan, M. Xu, L. Zeng, and Y. Qiao, "SpiderCNN: Deep learning on point sets with parameterized convolutional filters," in *European Conference on Computer Vision*, 2018.
- [159] Y. Wang, Y. Sun, Z. Liu, S. E. Sarma, M. M. Bronstein, and J. M. Solomon, "Dynamic graph cnn for learning on point clouds," *ACM Transactions On Graphics*, vol. 38, no. 5, pp. 1–12, 2019.
- [160] Y. Li, R. Bu, M. Sun, W. Wu, X. Di, and B. Chen, "PointCNN: Convolution on x-transformed points," in *Advances in Neural Information Processing Systems*, 2018.
- [161] H. Thomas, C. R. Qi, J.-E. Deschaud, B. Marcotegui, F. Goulette, and L. J. Guibas, "KPConv: Flexible and deformable convolution for point clouds," in *IEEE International Conference on Computer Vision*, 2019.
- [162] H. Zhao, L. Jiang, J. Jia, P. H. Torr, and V. Koltun, "Point transformer," in *IEEE International Conference on Computer Vision*, 2021.
- [163] Q. Hu, B. Yang, L. Xie, S. Rosa, Y. Guo, Z. Wang, A. Trigoni, and A. Markham, "RandLA-Net: Efficient semantic segmentation of large-scale point clouds," *IEEE Conference on Computer Vision and Pattern Recognition*, 2020.
- [164] Y. Zhang, Z. Zhou, P. David, X. Yue, Z. Xi, B. Gong, and H. Foroosh, "PolarNet: An improved grid representation for online lidar point clouds semantic segmentation," in *IEEE Conference on Computer Vision and Pattern Recognition*, 2020.
- [165] X. Zhu, H. Zhou, T. Wang, F. Hong, Y. Ma, W. Li, H. Li, and D. Lin, "Cylindrical and asymmetrical 3d convolution networks for lidar segmentation," in *IEEE Conference on Computer Vision and Pattern Recognition*, 2021.
- [166] R. Cheng, R. Razani, E. Taghavi, E. Li, and B. Liu, "(AF)2-S3Net: Attentive feature fusion with adaptive feature selection for sparse semantic segmentation network," in *IEEE Conference on Computer Vision and Pattern Recognition*, 2021.
- [167] M. Gerdzhev, R. Razani, E. Taghavi, and L. Bingbing, "TORNADO-Net: multiview total variation semantic segmentation with diamond inception module," in *IEEE International Conference on Robotics and Automation*, 2021.
- [168] V. E. Liong, T. N. T. Nguyen, S. Widjaja, D. Sharma, and Z. J. Chong, "AMVNet: Assertion-based multi-view fusion network for lidar semantic segmentation," *arXiv preprint arXiv:2012.04934*, 2020.
- [169] M. Ye, S. Xu, T. Cao, and Q. Chen, "DRINet: A dual-representation iterative learning network for point cloud segmentation," in *IEEE International Conference on Computer Vision*, 2021.
- [170] M. Ye, R. Wan, S. Xu, T. Cao, and Q. Chen, "Drinet++: Efficient voxel-as-point point cloud segmentation," *arXiv preprint arXiv:2111.08318*, 2021.
- [171] J. Xu, R. Zhang, J. Dou, Y. Zhu, J. Sun, and S. Pu, "RPVNet: A deep and efficient range-point-voxel fusion network for lidar point cloud segmentation," in *IEEE International Conference on Computer Vision*, 2021.
- [172] K. Genova, X. Yin, A. Kundu, C. Pantofaru, F. Cole, A. Sud, B. Brewington, B. Shucker, and T. Funkhouser, "Learning 3d semantic segmentation with only 2d image supervision," in *International Conference on 3D Vision*, 2021.
- [173] X. Yan, J. Gao, C. Zheng, C. Zheng, R. Zhang, S. Cui, and Z. Li, "2DPASS: 2d priors assisted semantic segmentation on lidar point clouds," *arXiv preprint arXiv:2207.04397*, 2022.
- [174] V. A. Sindagi, Y. Zhou, and O. Tuzel, "MVX-Net: Multi-modal voxelnet for 3d object detection," in *IEEE International Conference on Robotics and Automation*, 2019.
- [175] M. Liang, B. Yang, Y. Chen, R. Hu, and R. Urtasun, "Multi-task multi-sensor fusion for 3d object detection," in *IEEE Conference on Computer Vision and Pattern Recognition*, 2019.
- [176] M. Liang, B. Yang, S. Wang, and R. Urtasun, "Deep continuous fusion for multi-sensor 3d object detection," in *European Conference on Computer Vision*, 2018.
- [177] R. Nabati and H. Qi, "CenterFusion: Center-based radar and camera fusion for 3d object detection," in *Proceedings of the IEEE/CVF Winter Conference on Applications of Computer Vision*, 2021.
- [178] X. Chen, T. Zhang, Y. Wang, Y. Wang, and H. Zhao, "Futr3d: A unified sensor fusion framework for 3d detection," *arXiv preprint arXiv:2203.10642*, 2022.
- [179] Z. Yang, J. Chen, Z. Miao, W. Li, X. Zhu, and L. Zhang, "DeepInteraction: 3d object detection via modality interaction," *arXiv preprint arXiv:2208.11112*, 2020.
- [180] C. R. Qi, W. Liu, C. Wu, H. Su, and L. J. Guibas, "Frustum pointnets for 3d object detection from rgb-d data," in *IEEE Conference on Computer Vision and Pattern Recognition*, 2018.
- [181] J. Ku, M. Mozifian, J. Lee, A. Harakeh, and S. L. Waslander, "Joint 3d proposal generation and object detection from view aggregation," in *IEEE/RSJ International Conference on Intelligent Robots and Systems*, 2018.
- [182] S. Pang, D. Morris, and H. Radha, "CLOCs: Camera-lidar object candidates fusion for 3d object detection," in *IEEE/RSJ International Conference on Intelligent Robots and Systems*, 2020.
- [183] J. Phillion, A. Kar, and S. Fidler, "Learning to evaluate perception models using planner-centric metrics," in *IEEE Conference on Computer Vision and Pattern Recognition*, 2020.
- [184] (2022) ViDAR – Forward Visual Perception for Advanced Self-Driving . [Online]. Available: <https://43.132.128.84/productions/visualRadar>
- [185] Y. Zhou, Y. He, H. Zhu, C. Wang, H. Li, and Q. Jiang, "Monocular 3d object detection: An extrinsic parameter free approach," in *IEEE Conference on Computer Vision and Pattern Recognition*, 2021.
- [186] R. Bommasani, D. A. Hudson, E. Adeli, R. Altman, S. Arora, S. von Arx, M. S. Bernstein, J. Bohg, A. Bosselut, E. Brunskill, E. Brynjolfsson, S. Buch, D. Card, R. Castellon, N. Chatteerji, A. Chen, K. Creel, J. Q. Davis, D. Demszky, C. Donahue, M. Doumbouya, E. Durmus, S. Ermon, J. Etchemendy, K. Ethayarajh, L. Fei-Fei, C. Finn, T. Gale,

- L. Gillespie, K. Goel, N. Goodman, S. Grossman, N. Guha, T. Hashimoto, P. Henderson, J. Hewitt, D. E. Ho, J. Hong, K. Hsu, J. Huang, T. Icard, S. Jain, D. Jurafsky, P. Kalluri, S. Karamcheti, G. Keeling, F. Khani, O. Khattab, P. W. Koh, M. Krass, R. Krishna, R. Kuditipudi, A. Kumar, F. Ladhak, M. Lee, T. Lee, J. Leskovec, I. Levent, X. L. Li, X. Li, T. Ma, A. Malik, C. D. Manning, S. Mirchandani, E. Mitchell, Z. Munyikwa, S. Nair, A. Narayan, D. Narayanan, B. Newman, A. Nie, J. C. Niebles, H. Nilforoshan, J. Nyarko, G. Ogut, L. Orr, I. Papadimitriou, J. S. Park, C. Piech, E. Portelance, C. Potts, A. Raghunathan, R. Reich, H. Ren, F. Rong, Y. Roohani, C. Ruiz, J. Ryan, C. Ré, D. Sadigh, S. Sagawa, K. Santhanam, A. Shih, K. Srinivasan, A. Tamkin, R. Taori, A. W. Thomas, F. Tramèr, R. E. Wang, W. Wang, B. Wu, J. Wu, Y. Wu, S. M. Xie, M. Yasunaga, J. You, M. Zaharia, M. Zhang, T. Zhang, X. Zhang, Y. Zhang, L. Zheng, K. Zhou, and P. Liang, "On the opportunities and risks of foundation models," *arXiv preprint arXiv:2108.07258*, 2021.
- [187] T. Brown, B. Mann, N. Ryder, M. Subbiah, J. D. Kaplan, P. Dhariwal, A. Neelakantan, P. Shyam, G. Sastry, A. Askell, S. Agarwal, A. Herbert-Voss, G. Krueger, T. Henighan, R. Child, A. Ramesh, D. Ziegler, J. Wu, C. Winter, C. Hesse, M. Chen, E. Sigler, M. Litwin, S. Gray, B. Chess, J. Clark, C. Berner, S. McCandlish, A. Radford, I. Sutskever, and D. Amodei, "Language models are few-shot learners," in *Advances in Neural Information Processing Systems*, 2020.
- [188] P. Wang, A. Yang, R. Men, J. Lin, S. Bai, Z. Li, J. Ma, C. Zhou, J. Zhou, and H. Yang, "OFA: Unifying architectures, tasks, and modalities through a simple sequence-to-sequence learning framework," in *International Conference on Machine Learning*, 2022.
- [189] J. Zhu, X. Zhu, W. Wang, X. Wang, H. Li, X. Wang, and J. Dai, "Uni-Perceiver-MoE: Learning sparse generalist models with conditional moes," *arXiv preprint arXiv:2206.04674*, 2022.
- [190] S. Reed, K. Zolna, E. Parisotto, S. G. Colmenarejo, A. Novikov, G. Barth-Maron, M. Gimenez, Y. Sulsky, J. Kay, J. T. Springenberg, T. Eccles, J. Bruce, A. Razavi, A. Edwards, N. Heess, Y. Chen, R. Hadsell, O. Vinyals, M. Bordbar, and N. de Freitas, "A generalist agent," *arXiv preprint arXiv:2205.06175*, 2022.

## APPENDIX A

### MORE RELATED WORK

In this section, we describe 3D perception tasks and their conventional solutions, including monocular camera-based 3D object detection, LiDAR-based 3D object detection and segmentation and sensor-fusion-based 3D object detection.

#### A.1 Monocular Camera-based Object Detection

Monocular camera-based methods take an RGB image as input and attempt to predict the 3D location and category of each object. The main challenge of monocular 3D detection is that the RGB image lacks depth information, so these kinds of methods need to predict the depth. Due to estimating depth from a single image being an ill-posed problem, typically monocular camera-based methods have worse performance than LiDAR-based methods.

Mono3D [144] proposes a 3D proposal generation method with contextual and semantic information and uses an R-CNN-like architecture to predict the 3D boxes. Deep3DBox [145] predicts the 2D bounding box first, then estimate the 3D information from the 2D box, extending an advanced 2D detector. 3D-RCNN [146] also extends R-CNN in 2D detection, not only predicting the 3D bounding box but also rendering the shape of each object. CenterNet [147] is an anchor-free 2D detector and predicts the object center and the distance to the box. It can also easily extend to 3D detection by predicting the 3D size, depth, and orientation. Pseudo-Lidar [89] first predicts the depth map, then uses camera parameters to back-project the image with depth to the 3D point cloud in the LiDAR coordinate. Then any LiDAR-based detectors can be applied to the predicted “pseudo LiDAR”. The M3D-RPN [148] uses a single-stage 3D region proposal network, with two parallel paths for feature extraction: one global path with regular convolution, and one local depth-aware path using the non-shared Conv kernels in the  $H$  space. MonoPSR [149] first detects 2D boxes and inputs the whole image and the cropped objects, then two parallel branches are performed: a proposal generation module to predict the coarse boxes, and an instance reconstruction module to predict the mesh of the cropped object. In the second proposal refinement module, the reconstructed instance is used to get the refined 3D box. ROI-10D [150] predicts the 2D box and depth first, then lift them to 3D RoIs and uses RoIAlign to crop the 3D feature for regressing the 3D bounding box. It can also easily extend to 3D mesh prediction. SMOKE [83] is a one-stage anchor-free method that directly predicts the 3D center of the objects and the 3D box size and orientation. FCOS3D [82] is a recent representative monocular 3D detection method which extends the state-of-the-art 2D detector, FCOS [98]. The regression branch is similar to CenterNet; they all add the depth and the box size prediction in the regression branch. FCOS3D also introduces some tricks *e.g.* flip augmentation and test-time augmentation. PGD [62] analyzes the importance of depth estimation in the monocular 3D detection and then proposes a geometric relation graph to capture the relation of each object, resulting in better depth estimation.

#### A.2 LiDAR Detection and Segmentation

LiDAR describes surrounding environments with a set of points in the 3D space, which capture geometry information of objects. Despite the lack of color and texture information and the limited perception range, LiDAR-based methods outperform camera-based methods by a large margin benefit from depth prior.

##### A.2.1 Detection

As data collected by LiDAR is formatted as point clouds, it is natural to construct neural networks directly on points. Point-based methods process on raw point cloud data to conduct feature extraction. VoteNet [118] directly detects objects in point clouds based on Hough voting. PointRCNN [151] is a two-stage method for more accurate 3D detection. In the first stage, 3D proposals are generated via segmenting the point cloud into foreground and background points, and then proposals are refined to obtain the final bounding boxes in the second stage. Part-A<sup>2</sup> [152] extends PointRCNN with the part-aware and neural aggregation network. H3DNet [153] predicts a hybrid set of geometric primitives, which are then converted to object proposals by defining a distance function between an object and the geometric primitives. A drawback of voting methods is that outlier votes from backgrounds hurt the performance. Pointformer [119] designs a Transformer backbone, which consists of Local Transformer and Global Transformer, to learn features effectively. BRNet [154] back-traces the representative points from the vote centers and revisits complementary seed points around these generated points. Instead of grouping local features, Group-Free [155] obtain the feature of an object from all the points using an attention mechanism. RBGNet [156] proposes a ray-based feature grouping module to learn better representations of object shapes to enhance cluster features. 3DSSD [157] first presents a lightweight and effective point-based single-stage 3D detector. It utilizes 3D Euclidean distance and Feature-FPS as sampling strategy.

##### A.2.2 Segmentation

Besides 3D object detection, the task of point cloud segmentation provides the whole scene understanding from point cloud data. Some works focus on indoor point cloud segmentation. PointNet [102] provides a unified operator by combining MLP and max pooling to learn point-wise features directly from point clouds. PointNet++ [103] further introduces set abstraction to form a local operation for more representative feature extraction. SpiderCNN [158] proposes a novel convolutional architecture for efficient geometric feature extraction. DGCNN [159] proposes EdgeConv to learn incorporates local neighborhood information. PointCNN [160] uses  $X$ -transformation to simultaneously weight and permute the input features for subsequent convolution on the transformed features. KPConv [161] stores convolution weights in Euclidean space by kernel points, which are applied to the input points close in the neighborhood. Point Transformer [162] is a Transformer-based method that designs self-attention layers for the point cloud.

Different from indoor scene segmentation, outdoor segmentation models are designed for more imbalance point

distribution. RandLA-Net [163] uses random point sampling instead of complicated point selection methods for efficient and lightweight architecture. PolarNet [164] uses polar BEV representation to balance the number of points across grids. Cylinder3D [165] introduces a novel cylindrical partition voxelization method and asymmetrical 3D convolution networks to ease the problem of imbalance point distribution. (AF)<sup>2</sup>-S3Net [166] fuses the voxel-based and point-based learning methods into a unified framework by the proposed multi-branch attentive feature fusion module and adaptive feature selection module. TornadoNet [167] incorporates bird-eye and range view feature with a novel diamond context block. AMVNet [168] aggregates the semantic features of individual projection-based networks. DRINet [169] designs architecture for dual-representation iterative learning between point and voxel. DRINet++ [170] extends DRINet by enhancing the sparsity and geometric properties of a point cloud. Sparse Point-Voxel Convolution (SPVConv) [84] uses an auxiliary point-based branch to preserve high-resolution features from voxelization and aggressive downsampling. Information exchanges are performed in different stages of the network between the point-based and voxel-based branches. RPNNet [171] devises a deep fusion network with multiple and mutual information interactions among voxel-, point-, and range-view. 2D3DNet [172] uses labeled 2D images to generate trusted 3D labels for network supervision. 2DPASS [173] boosts the point clouds representation learning by distilling image features into the point cloud network.

### A.3 Sensor Fusion

Modern autonomous vehicles are equipped with different sensors such as cameras, LiDAR and Radar. Each sensor has advantages and disadvantages. Camera data contains dense color and texture information but fails to capture depth information. LiDAR provides accurate depth and structure information but suffers from limited range and sparsity. Radar is more sparse than LiDAR, but has a longer sensing range and can capture information from moving objects. Ideally, sensor fusion will push the performance upper bound of the perception system, but how to fuse the data from different modalities is a challenging problem.

MVX-Net [174] projects the voxel region to the image and applies ROI Pooling to extract the image feature. MMF [175] and ContFuse [176] project LiDAR points from each BEV feature to the image feature map and apply the continuous convolutions to fuse the feature. PointAugmenting [122] constructs image feature point clouds by projecting all LiDAR points to image features. The fused feature is obtained by concatenation of two BEV features from LiDAR feature point clouds and image feature point clouds after the 3D backbone. AutoAlignV2 [78] utilizes the deformable attention [135] to extract the image feature with LiDAR feature after projecting the LiDAR point to image as reference point. DeepFusion [77] applies the transformer [95] for fusion by using the voxel feature as query and image feature as key and value. CenterFusion [177] uses the frustum association to fuse the radar feature and image feature with preliminary 3D boxes. FUTR3D [178] projects the 3D reference points to feature maps from different modalities and fuses features

using deformable attention. TransFusion [76] uses a spatially modulated cross attention to fuse the image features and the LiDAR BEV features, to involve the locality inductive bias. DeepInteraction [179] preserves modal-specific representations instead of a single hybrid representation to maintain modal-specific information.

Besides fusing features from different modalities in the middle of neural networks, early fusion methods augment the LiDAR input with the aid of image information. PointPainting [73] concatenates the one-hot label from the semantic segmentation to point features according to the projection relationship. Then the augmented point feature is fed to any LiDAR-only 3D detector. F-PointNet [180] utilizes the 2D detector to extract the point cloud within the viewing frustum of each 2D bounding box. Then each viewing frustum with the corresponding point cloud is fed to a LiDAR-only 3D detector.

Late fusion methods fuse the multi-modal information after the generation of object proposals. MV3D [108] takes the BEV, front view LiDAR, and image as input. After obtaining the 3D proposals from BEV and projecting 3D proposals to other modalities, features from different modalities of the same 3D proposal are fused to refine proposals. AVOD [181] improves the MV3D [108] with high resolution image feature. CLOCs [182] operate on the prediction results from the 2D and 3D detector with a small network to adjust the confidence of the pair-wise 2D and 3D with non-zero IoU.

## APPENDIX B

### PRELIMINARY IN 3D VISION

#### B.1 Mathematical Formulation in 3D Vision

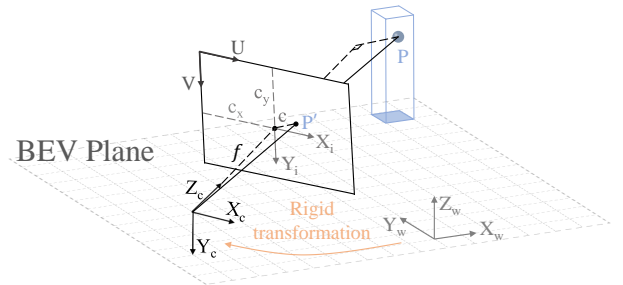


Fig. 7: View transformation from perspective view to bird's-eye-view (BEV). The  $(X_w, Y_w, Z_w)$ ,  $(X_c, Y_c, Z_c)$  represent world coordinate and camera coordinate, and the  $(X_i, Y_i)$ ,  $(U, V)$  represent image coordinate and pixel coordinate. A pillar is lifted from the BEV plane.  $P, P'$  corresponds to the 3D point from the pillar and the projected 2D point from the camera view, respectively. Given the world coordinates of  $P$  and the intrinsic and extrinsic parameters of the camera, the pixel coordinates of  $P'$  can be obtained.

Explicit BEV feature construction typically requires indexing local image-view features based on 3D-to-2D projection. Fig. 7 depicts the view transformation in BEVFormer [4]. A pillar is lifted from the BEV plane, and a 3D point inside the pillar is projected to the camera view. The

projection process involves the transformation between the world, camera, image, and pixel coordinate systems.

The transformation from the world coordinate to the camera coordinate is a rigid transformation, requiring translation and rotation only. Let  $P_w = [x_w, y_w, z_w, 1]$ ,  $P_c = [x_c, y_c, z_c, 1]$  be the homogenous representations for a 3D point  $P$  in the world coordinate and the camera coordinate respectively. Their relation can be described as follows:

$$P_c = \begin{bmatrix} x_c \\ y_c \\ z_c \\ 1 \end{bmatrix} = \begin{bmatrix} \mathbf{R} & \mathbf{T} \\ \mathbf{0}^T & 1 \end{bmatrix} \begin{bmatrix} x_w \\ y_w \\ z_w \\ 1 \end{bmatrix}, \quad (12)$$

where  $\mathbf{R}$ ,  $\mathbf{T}$  refers to a rotation matrix and a translation matrix respectively.

The image coordinate system is introduced to describe the perspective projection from the camera coordinate system onto the image. When not taking the camera distortion into consideration, the relationship between a 3D point and its projection on image plane can be simplified as a pinhole model. The image coordinates  $(x_i, y_i)$  can be calculated by Eqn. 13:

$$\begin{cases} x_i = f \cdot \frac{x_c}{z_c} \\ y_i = f \cdot \frac{y_c}{z_c} \end{cases}, \quad (13)$$

where  $f$  represents the focal length of camera.

There is a translation and scaling transformation relationship between the image coordinate system and the pixel coordinate system. Let us denote  $\alpha$  and  $\beta$  representing the scale factors to the abscissa and the ordinate, and  $c_x$ ,  $c_y$  representing the translation value to the coordinate system origin. The pixel coordinates  $(u, v)$  is mathematically represented by Eqn. 14:

$$\begin{cases} u = \alpha x + C_x \\ v = \beta y + C_y \end{cases}. \quad (14)$$

With Eqn. 13 and Eqn. 14, setting  $f_x = \alpha f$ ,  $f_y = \beta f$ , we could derive Eqn. 15:

$$z_c \begin{bmatrix} u \\ v \\ 1 \end{bmatrix} = \begin{bmatrix} f_x & 0 & c_x \\ 0 & f_y & c_y \\ 0 & 0 & 1 \end{bmatrix} \begin{bmatrix} x_c \\ y_c \\ z_c \end{bmatrix}. \quad (15)$$

In summary, the relationship between the 3D point  $P$  in the world coordinate system and its projection  $P'$  in the pixel coordinate system can be described as:

$$z_c \begin{bmatrix} u \\ v \\ 1 \end{bmatrix} = \begin{bmatrix} f_x & 0 & c_x \\ 0 & f_y & c_y \\ 0 & 0 & 1 \end{bmatrix} [\mathbf{R} \quad \mathbf{T}] \begin{bmatrix} x_w \\ y_w \\ z_w \\ 1 \end{bmatrix}, \quad (16)$$

$$= \mathbf{K} [\mathbf{R} \quad \mathbf{T}] [x_w \quad y_w \quad z_w \quad 1]^T.$$

The matrix  $\mathbf{K} = \begin{bmatrix} f_x & 0 & c_x \\ 0 & f_y & c_y \\ 0 & 0 & 1 \end{bmatrix}$  is termed as the camera intrinsics, and the matrix  $[\mathbf{R} \quad \mathbf{T}]$  is called as the camera extrinsics. With the world coordinates of 3D points, the camera intrinsics and extrinsics, the projections on the image view can be obtained by aforementioned transformation.

## APPENDIX C

### DATASET AND EVALUATION METRICS

#### C.1 Argoverse Dataset

Argoverse [12, 24] is the first self-driving dataset with HD-Map. The sensor set of Argoverse contains 2 LiDARS, 7 ring cameras, and two stereo cameras. The early version, termed Argoverse 1 [24], supports two tasks: 3D tracking and motion forecasting. And the new Argoverse 2 [12] supports more tasks: 3D object detection, unsupervised learning, motion prediction and changed map perception, which is more diverse and challenging.

#### C.2 Evaluation Metrics

**PKL.** Planning KL-Divergence (PKL) is a new neural planning metric proposed in CVPR 2020 [183], which is based on the KL divergence of the planner's trajectory and the route of the ground truth. The planner's trajectory is generated by giving the detection results from the trained detectors. The PKL metric is always non-negative. The smaller PKL scores mean the detection performance is better.

The localization affinity of LET-3D-APL is defined as:

- If no longitudinal localization error, the localization affinity = 1.0.
- If the longitudinal localization error is equal to or exceeds the maximum longitudinal localization error, the localization affinity = 0.0.
- The localization affinity is linearly interpolated between 0.0 and 1.0.

## APPENDIX D

### INDUSTRIAL VIEW ON BEV

Here we depict in detail the input and network structure in BEV architecture from different companies in Tab. 8.

## APPENDIX E

### CHALLENGES AND FUTURE TRENDS

Despite the popularity of BEV representation for perception algorithms in autonomous driving, there are still many grand challenges facing the community to resolve. In this section, we list some future research directions.

#### E.1 Depth Estimation

As discussed in main paper, the core issue for vision-based BEV perception lies in an accurate depth estimation, as the task is performed in 3D context. Current approaches to resolve depth prediction is (a) pseudo-LiDAR generation; (b) lifting features from 2D to 3D correspondence; (c) LiDAR-camera distillation; and (d) stereo disparity or temporal motion. Either one or a combination of these directions are promising. To guarantee better performance, the large-scale amount of supervision data is of vital importance as well [81].

Another interesting and important direction is how to utilize LiDAR information during training (e.g. as depth supervision), whilst only vision inputs are fed during inference. This is desperately favorable for OEMs as often we have convenient amount of training data from multiple sources and yet for the deployment consideration, only camera inputs are available on shipping products.

TABLE 8: Detailed input and network options for BEV architectures. As we can observe, modality and feature extractor are different; Transformer and ViDAR are the most common choice for BEV transformation in industry. “-” indicates unknown information.

Company	Modality			Feature Extractor	BEV Transformation	Temporal & Spatial Fusion
	Camera	LiDAR	IMU/GPS			
Tesla [6]	✓	✗	✓	RegNet+BiFPN	Transformer ViDAR	✓
Mobileye (SuperVision) [128]	✓	✓	-	-	ViDAR	-
Horizon Robotics [125]	✓	✓	✓	-	Transformer	✓
HAOMO.AI [126]	✓	✓	✓	ResNet+FPN Pillar-Feature Ne	Transformer	✓
PhiGent Robotics [184]	✓	✗	✗	-	ViDAR	-

## E.2 Fusion Mechanism

Most fusion approaches up to date can be classified as one of the early-fusion, middle-fusion or late-fusion groups, depending on where the fusion module lies in the pipeline. The most straightforward design of sensor fusion algorithms is to concatenate two set of features from camera and LiDAR respectively. However, as previous sections articulate, how to “align” features from different sources is of vital importance. This means: (a) the feature representation from camera is appropriately depicted in 3D geometry space rather than 2D context; (b) the point clouds in 3D space have accurate correspondence with those counterparts in 2D domain, implying that the soft and/or hard synchronization between LiDAR and camera is exquisitely guaranteed.

Built on top of the prerequisites aforementioned, how to devise an elegant fusion scheme needs much more focus from the community. Future endeavors on this part could be, (a) utilizing self and/or cross attention to integrate feature representations from various modalities in Transformer spirit [14]; (b) knowledge from the general multi-modality literature could be favorable as well, e.g., the philosophy of text-image pairs in CLIP formulation [18] could inspire the information integration of different sensors in the autonomous driving domain.

## E.3 Parameter-free Design to Improve Generalization

One of the biggest challenges in BEV perception is the domain adaptation. How well the trained model in one dataset would behave and generalize in another dataset. One cannot afford the heavy cost (training, data, annotation, etc.) of the algorithm in each and every dataset. Since BEV perception is essentially a 3D reconstruction to the physical world, we argue that a good detector must bundle tight connection to camera parameters, esp. the extrinsic matrix. Different benchmarks have different camera/sensor settings, corresponding to physical position, overlap area, FOV (field-of-view), distortion parameters, etc. These factors would all contribute to the (extreme) difficulty of transferring good performance from one scenario to another domain.

To this end, it urges us to decouple the network from camera parameters, aka, making the feature learning independent of the extrinsic and/or intrinsic matrix. There are some interesting work in this direction both from academia (extrinsic free, [185]) and industry (rectify module, [6]). This is non-trivial nonetheless and it would be better to

investigate more from the community as future work. The parameter-free design is robust to resolve detection inaccuracy due to road bumpiness and camera unsteadiness in realistic applications.

## E.4 Foundation Models to Facilitate BEV Perception

There is blossom in recent years from the general vision community where large or foundation models [14, 15, 18, 186, 187] achieve impressive performance and override state-of-the-arts in many domains and tasks. At least two aspects are worth investigating for BEV perception.

One is to apply the affluent knowledge residing in the large pre-trained models and to provide better initial checkpoints to finetune. However, the direct adaptation of some 2D foundation model might not work well in 3D BEV sense, as previous section implies. How to design and choose foundation models to better adapt autonomous driving tasks is a long standing research issue we can embrace.

Another unfinished endeavor is how to develop the idea of multi-task learning as in the foundation models (generalist) for BEV perception. There are interesting work in the general vision literature where OFA [188], Uni-perceiver-MoE [189], GATO [190], etc. would perform multiple complicated tasks and achieve satisfying results. Can we apply the similar philosophy into BEV perception and unify multiple tasks in one single framework? This is meaningful as the perception and cognition domains in autonomous driving need collaborating to handle complicated scenarios towards the ultimate L5 goal.

## AUTHOR CONTRIBUTIONS

H. Li, J. Dai and L. Lu lead the project, provide mentorship and allocate resources across task tracks. H. Li, W. Wang, L. Lu drafted the main outline of the project, worked on a preliminary version of the manuscript, supervised key milestones of the project. H. Deng, H. Tian, X. Jia and B. Yu served as team lead for Camera-only Detection, LiDAR Segmentation, Motion Prediction, Occupancy Prediction track respectively. C. Sima, H. Wang, Z. Li, H. Deng, H. Tian, L. Chen and J. Yang are core members during the Challenge, implementing ideas, running experiments, responsible for key outputs of each track. Y. Gao implemented the model ensemble part and improved the performance to a great extent. Y. Li is in charge of the whole data processing team. X. Geng analysed the industrial pipeline design; J. Zeng

wrote the 3D preliminary section; E. Xie wrote and revised the dataset and evaluation part in the paper, discussed key ideas of BEVFormer work. Y. Qiao was the primary consultant, eliciting key goals and tracking progress. D. Lin, S. Liu and J. Yan advised on general picture of the research and gave additional comment on the manuscript. X. Zhu, J. Shi, and P. Luo oversaw the project from their inception.